MULTIPLE APPROACHES TO CHARACTERIZING PORE STRUCTURE FOR A RANGE OF SANDSTONE SAMPLES

by

SAMSON S. ARAWOLE

Presented to the Faculty of the Graduate School of

The University of Texas at Arlington in Partial Fulfillment

of the Requirements

for the Degree of

MASTER OF SCIENCE IN GEOLOGY

THE UNIVERSITY OF TEXAS AT ARLINGTON

August 2015

Acknowledgements

First of all I thank GOD Almighty for making this possible and my pastor, Pastor Joseph Popoola of Sure Foundation Ministries, for his spiritual support and prayer.

I also thank the management and staff of Core Laboratories Advanced Technology Center in Houston for allowing the use of the company resources. Especially instructive is the assistance of Robert Lee, the current Manager for USA Operations. I am grateful to Jerry Warne (my life-time manager for core analysis). Special thanks go to AJ Kumar (Digital Rock Physics Manager) and Derrick Beckett (Director of Technology Development) for Micro Ct Scan; Tuan Vo and his team for helping with NMR; Phil Hawley, Casey Markey and the group for MICP; Jasmine Langston and the Flow Studies team for helping with brine permeability and sample testing. Thumbs up for Joe Davis for running the liquid perm!!!

Special thanks go to Dr. Dan Gostovic (FEI Visualization Sciences Group) for providing the license of Avizo Fire for processing Ct Scans and Dr. Arash Aghaei for providing clarifications and enhancing valuable paths of understanding.

My gratitude goes to my supervising professor, Dr. Qinhong Hu, for his criticisms and engagement. Special thanks go to Drs. Wickham and Griffith for valuable inputs as advising committee members. I am especially grateful to Dr. Wickham for all his critical but fatherly advice and guidance throughout my education at UT Arlington. Thank you all!. I acknowledge my friend, brother and colleague Bolaji Oloyede. Your encouragement and persistence is appreciated. God bless you and your family. Finally I am very grateful for the support of my wife and friend, Abioye Abiola Abolanle Arawole and members of our dynasty, Moses, Christopher, Gabriel and Bella (our little Chiweenie). Thank you all.

August 17, 2015

Abstract

MULTIPLE APPROACHES TO CHARACTERIZING

PORE STRUCTURE FOR A RANGE OF

SANDSTONE SAMPLES

Samson S. Arawole, MS

The University of Texas at Arlington, 2015

Supervising Professor: Qinhong Hu

Using various approaches, this work examines pore structure (geometry and connectivity) of a range of sandstone samples with their permeability varying by five orders of magnitude. The following four experimental approaches were used: Mercury Injection Capillary Pressure (MICP), Nuclear Magnetic Resonance (NMR), Fluid imbibition and Micro Ct Scan imaging. Fluid imbibition was used to gauge pore connectivity of these sandstones. Furthermore, basic properties of air porosity and permeability were obtained on the samples before and after all four procedures and used as a basis for property comparison. “Specific” API brine permeability was also run on all samples for comparison as well as a verification of the sample’s reaction to fluid.

While pore throats were extracted from mercury injection, pore bodies were drawn from nuclear magnetic resonance. Both of these results were compared with pore throats and pore bodies generated from the processed Ct Scan images. Average pore throat and pore body sizes were also enumerated from NMR, MICP and Micro Ct Scan tests, and the results complement each other. The results of total porosity, permeability

and pore size distribution were obtained and they compare well among several approaches.

Pore size distribution, pore throat distribution and coordination numbers from NMR, XCT and MICP were displayed by frequency distribution diagrams and analyzed. According to the results, the sample with the highest permeability (Idaho Gray sandstone) has the longest T_2 time from NMR, highest throat size from MICP and Ct scan, and highest average pore size and coordination number from Ct Scan. This sample also has the least entry pressure from MICP test.

Across all samples, the results show a direct correlation between high permeability and long T_2 relaxation time from NMR, a high average coordination number from Ct scan and large throat from MICP, confirming connectivity, and a low intrusion entry pressure from MICP, also confirming connectivity according to Washburn equation 3-1.

The high-permeability Boise sandstone is frequently discussed throughout the thesis because it is one of the samples on which all four experimental approaches have been used. From Ct scans tests, Boise has a single peak or mono-modal, pore-size distribution curve, while two medium-permeability samples of Bandera Gray and Parker sandstones both have dual peaks.

Fluid imbibition also shows a standard slope of 0.5 or more for high permeability samples (a typical Fickian behavior).

All data collected indicate they could be correlated with connectivity and hence fluid flow in reservoir evaluation.

Overall results of this integrated study demonstrate that the procedures highly complement each other despite the different principles and methodologies behind them.

Table of Contents

List of Illustrations

List of Tables

List of Equations

Chapter 1

INTRODUCTION

The characterization of pore structure (both geometry and topology) in reservoir rocks and many other porous media is of fundamental importance for accurate evaluation of reservoir resources, petroleum recovery, as well as for environmental remediation and many chemical engineering processes. Methods to quantitatively characterize pore structure can be broadly classified into two groups (Hu et al., 2012): (1) direct imaging methods which include Back Scattered Scanning Electron Microscopy, X-ray Computed Tomography (XCT), and Focus Ion Beam Nano-tomography (FIB-nt); (2) indirect pore geometry/structure probes which include gas adsorption/condensation (N_2 or water vapor), Mercury Injection Capillary Pressure (MICP), and Nuclear Magnetic Resonance (NMR) relaxometry.

For measuring pore size distribution and other critical petrophysical parameters, several companies, end-users and vendors are limited on which tests or options to choose due to limited knowledge of procedure, budget restriction, and project deadline; plain vendor marketing is sometimes the deciding factor for most companies to select which procedure to follow.

The motivation and objective of this work is to investigate pore structure (i.e., pore size distribution, connection and other critical parameters) of seven sandstone samples using MICP, NMR, Micro-XCT and fluid imbibition tests. Results of this study will add to the body of knowledge about pore structure of different sandstones, and lead to better knowledge of anticipated results when a specific methodology or approach is applied to pore structure investigation. Method comparison will increase our knowledge on how all the procedures compare, and clarify what parameters are derived from which procedure or what procedure is better suited for a particular parameter. The use of

commonly used samples that are homogeneous help reduces the ambiguity that may be associated with non-homogeneous and samples containing clays.

Chapter 2

BASIC PROPERTIES OF SAMPLES

Seven 1.5”×6” sandstone samples, with a range of porosity (7-29%; Table 2-1) and permeability (0.12-7500 mD), were purchased from Kocurek industries, Caldwell, TX. See Figure 2-1 for pictures, and Table 2-1 for the basic properties provided by Kocurek Industries. Table 2-2 shows basic properties as measured in the lab prior to procedures.

The samples, according to Kocurek, come primarily from the Appalachian Basin. There the Berea sandstone of eastern Ohio, western Pennsylvania, western West Virginia, and eastern Kentucky have long been an important producer of oil and gas. The exception is Crab Orchard, which is a part of Crab Orchard Mountains Group of Tennessee.

Figure 2-1: Samples “as received” from Kocurek Industries

Table 2-1: Reported basic properties from Kocurek Industries (listed with a decreasing air permeability)

Sample information as received from Kocurek

Name	Formation	Porosity Fraction	Est. Air Perm (mD)	Est. Brine Perm (mD)	Confining Stress (psi)	Homogeneity
Idaho Gray	Idaho	.29	7500	2200	3500	YES
Boise	Idaho	.28	1575-2040	473-612	4000	YES
Gray Berea	Kipton	0.19-0.20	200-315	60-100	6500-8000	YES
Bandera Gray	Kansas	.21	30	8	5000	YES
Parker	Edwards Plateau	.17	30	9	10000	NO
Kentucky	Kentucky	.14	1-5	0.1 - 1	8000	YES
Crab Orchard	Tennessee	0.07	0.12	0.01-0.1	25000	YES

Table 2-2 Measured basic properties before procedures.

Sample Basic Properties as measured in Core Laboratories

Name	Formation	Porosity Fraction	Est. Air Perm (mD)	Est. Brine Perm (mD)	Confining Stress (psi)	Homogeneity
Idaho Gray	Idaho	.32-.33	29830 - 30000	22100	800	NA
Boise	Idaho	.28	4750-5450	5400	800	NA
Gray Berea	Kipton	.20	166-182	104	800	NA
Bandera Gray	Kansas	.20	18.5-26.2	12.9	800	NA
Parker	Edwards Plateau	.183	22.8-24.6	9.6	800	Na
Kentucky	Kentucky	.144	.522-.633	0.149	800	Na
Crab Orchard	Tennessee	0.073	0.027-0.028	0.00337	800	NA

Chapter 3

METHODS

Seven sandstone samples were prepared according to API RP 40 Standards. They were quarried and drilled samples, so no sample cleaning was necessary. Each sample was weighed and photographed “as received’. They were then cut into two 1.5”×3” sets with subscripts A and B. Set A was used to conduct MICP, CT Scan, NMR and liquid permeability experiments at Core Laboratories facilities in Houston TX, while Set B was used for fluid imbibition at the Reservoir Characterization Laboratory of the University of Texas at Arlington.

Average sample size of 1.5”x 2.8” was used for basic property measurements for all fourteen samples. Before measuring basic properties, all samples were prepared according to API RP 40 Standards by drying in conventional oven at 240^{o}F (115.5^{o}C) for a minimum of 48 hours. They were cooled in a desiccator before weighing, and repeated weights were taken to confirm weight consistency. After that, basic properties of helium porosity, grain volume using Boyle’s Law, and air permeability using CMS 300 were conducted on all fourteen samples.

Small (1” × 1.5” diameter) trims were cut from the Set A samples. From these trims, sample sizes of 1” × 0.8” were further drilled out for MICP tests and 5mm × 5mm × 5mm cubes cut out for Micro Ct Scan experiments. The remaining 2” × 1.5” diameter samples were retained for API brine permeability and NMR tests.

The Set B samples were prepared into cylindrical samples of 2” × 1.5” and cubes of 1cm × 1cm × 1cm for fluid imbibition using de-ionized water.

3.1 Principles of Mercury Injection Capillary Pressure (MICP):

MICP is an important and established characterization technique for porous materials. Pores between 500 micron meters (μm) and 3.0 Nano-meters (nm) in diameters can be investigated by MICP approach. This dynamic technique is based on the intrusion of non-wetting mercury into porous structure under controlled pressures. The non-wetting characteristic and high surface tension makes mercury ideal for pore structure investigations.

Mercury intrusion into porous materials allow for the evaluation of numerous sample properties such as capillary pressure trend, pore-throat distribution, median pore throat diameter, total pore volume or porosity, skeletal density, bulk density and seal capacity. Several attempts have also been used to determine particle size distribution from mercury intrusion according to Mayer-Stowe theory (Carlos A. Le´on y Le´on., 1998).

Also called mercury intrusion porosimetry, MICP is based on the capillary law governing liquid penetration into small pores. As a non-wetting fluid to most porous media and because of its high surface tension, mercury will not spontaneously invade pores by a capillary action unless an external pressure is applied. It invades pore throats by overcoming the capillary pressure through an applied external pressure of up to 60,000 psia (413 MPa). The required equilibrated pressure is inversely proportional to the size of pore-throat invaded, and is used to generate their volume and size distribution using the modified Young-Laplace equation, which is also referred to as Washburn equation (Equation 3.1). A key assumption in the equation is that all pores have a cylindrical geometry.

$$\Delta \mathbf{P} = -\left(\frac{2\gamma \cos \theta}{\mathbf{R}}\right) \quad \text{..... (3-1)}$$

Where,

ΔP = pressure difference across the curved mercury interface (psia);

ϒ = surface tension of mercury (485 dynes/cm);

θ = contact angle between mercury and the porous medium (140 degrees);

R = corresponding pore-throat radius (μm).

Although pores are rarely cylindrical in reality, this equation provides a practical representation of pore distributions and yields very useful and applicable results for most applications.

Micrometrics Auto pore IV 9520, located at Core Laboratories, Advanced Technology Center, Houston TX, was used for MICP tests of this work (Figure 3.1). During sample analysis, MICP collects the data of applied pressure via several transducers, and mercury intrusion volume at specific pressures using a capacitance measurement between the metal shield on the outside of a glass capillary (penetrometer) and the length of the mercury column in the same capillary. Penetrometer size is selected based on sample pore volume, with the amount of intruded mercury volume readily detected.

Figure 3-1: Mercury Injection Capillary Pressure (MICP) equipment.

Furthermore, absolute permeability values of porous media can also be calculated from MICP analyses using several algorithms, including Purcell (Purcell, 1949), Thomeer (Thomeer, 1960) , Swanson (Swanson, 1981), and Katz and Thompson (c.f., Gao and Hu, 2013).

Swanson method of permeability calculation was adopted for this work. Swanson method can be correlated to air or brine permeability but this work adopted a correlation to air permeability as depicted in the equation below (Equation 3.2)

$Ka = 399 * (Max\ \frac{Sb}{Pc})$^1.691 ..... (3-2) (Swanson, 1981)

Or

$Kw = 431 * (Max\ \frac{Sb}{Pc})$^2.109.....(3-2a) (Newsham et al., 2007)

Where, K_a = permeability to air (md)

K_w = permeability to water (md)

S_b = mercury saturation (fraction)

P_c = mercury capillary pressure (psia)

Max $(S_b/P_c)_A$ = the ratio of S_b and P_C is at the maximum at point “A” using Thomeer hyperbola and therefore allowing for permeability calculation with the equation above (Swanson, 1981)

3.1.1 Procedure for MICP Analyses:

Each sample was oven-dried at 240 °F for at least 48 hours to remove moisture, and then cooled to room temperature in a desiccator and a weight taken before the MICP test. To perform an analysis, the sample is loaded into a penetrometer which consists of a sample chamber, connected to a metal-clad, precision-bore and glass capillary stem. The penetrometer is sealed and placed in a low pressure chamber where the sample is evacuated to 50 μm Hg (0.05 torr, 0.000972 psi, or 6.7 Pascal) to remove excess air and moisture. During the MICP test, each sample undergoes both low-pressure and high-pressure analyses. Under low-pressure analysis, the mercury fills up the sealed sample cup. A maximum filling pressure of 0.58 psia (conformance pressure), and equilibrium time (the minimum time duration to achieve stable mercury level before proceeding to the next pressure) of 30 seconds, was set for low-pressure analyses of the samples. Mercury first fills up pore spaces that can easily be accessed by overcoming the capillary pressure of larger pore-throats with a limit of about 300 μm (depending on the filling pressure used) for low-pressure analysis.

For high-pressure analysis, mercury can intrude into pore throats as small as 3 nm at an incremental pressure from 1.2 psia (end of low-pressure) to 60,000 psia at the equilibrium time of 60 seconds. By measuring the volume of mercury that intrudes into the sample material with each pressure change, and knowing the values of interfacial tension of mercury and contact angle between mercury and rock sample for Washburn equation, values of pore-throat radius, porosity, and permeability are obtained (Gao and Hu, 2012; Hu and Ewing., 2014). After mercury intrusion, a step-wise mercury extrusion was also performed to mimic fluid (air) imbibition process and to evaluate the issue of hysteresis.

3.2 Principles of Nuclear Magnetic Resonance (NMR):

Hydrogen proton Nuclear Magnetic Resonance (NMR) is a non-destructive measurement technique that can provide a wealth of information regarding pores, as well as its fluid content and type, within a reservoir rock. The measurement is obtained by manipulating the electrically-charged hydrogen nuclei within the magnetic field. Essentially rock-core NMR is used to determine the hydrogen bearing content of a rock sample, and the three fluids (oil, water and gas) that occupy a reservoir are hydrogen bearing.

Hydrogen protons which have an inherent spin about their axis are normally randomly aligned according to a local magnetic field. An applied static magnet and radio frequency pulse according to Lamor frequency forces them to polarize and then precess. This precession generates an exponential decay, which is mathematically converted to a T_2 transverse relaxation time through a process of inversion. The Carr-Purcell-Meiboom-Gill (CPMG) pulse sequence produces a closely-spaced train of spin echoes, and its decay is analyzed to determine T_2. Spin echo is the signal induced on the receiver when hydrogen protons re-phase by a short 180^0 magnetic pulse at the Lamor frequency.

There are generally two fields of NMR measurement: high field and low field. The low field NMR, used in laboratories for core tests, measures the following three properties: the equilibrium nuclei magnetization Mn, and the two principal NMR relaxation times (T_1, longitudinal relaxation time; T_2, the transverse relaxation time). Parameter Mn is proportional to the fluid-filled porosity, while T_1 and T_2 are correlated with petrophysical properties such as pore size, producible fluid and permeability.

There are three T_2 relaxation mechanisms in rocks, and they are (1) molecular motion in fluids, (2) surface relaxivity in the pore walls, and (3) molecular diffusion in the internal gradients. Called “bulk liquid relaxation”, the first mechanism which is due to collision between two hydrogen protons is equally effective whether or not the fluid is in a

rock. Bulk liquid T_2 is affected by the viscosity, temperature, and chemical composition of fluid. Bulk liquid typing finds its application in separating the fluids of oil, gas and water. The second relaxation mechanism, termed as “surface relaxation”, happens between hydrogen proton and grain surface, wherein pore size can be deduced. The third relaxation mechanism is due to the diffusion of molecules in magnetic field gradients. In laboratory NMR experiments, there is no gradient effect.

In water-saturated rocks, the bulk water relaxation is often negligible, and majority of the distribution of T_2 arises from the distribution of surface-to-volume ratio (S/V) of the pores (surface interaction), according to equation below (equation 3.3).

$$V/S = \rho_2 * T_2 \quad \text{..... (3-3)}$$

Where V/S = Ratio of volume to surface area of the pore (equivalent to pore size in μm)

ρ_2 = surface relaxivity (m/s)

T_2 = transverse decay time (ms)

Volume to Surface area (V/S) has been correlated to pore size (Looyestijn, 2001). Because T_2 depends linearly upon pore size, the T_2 distribution corresponds to a pore size distribution whereby the largest pore has the longest relaxation time and vice versa. Like MICP, current models for the analysis of the NMR T_2 data implicitly assume that the connected pore space can be represented by a bundle of capillaries in which the flow paths are parallel and controlled by the smallest diameter (pore throat) along the flow path.

The T_2 distribution curve is used for interpreting pore size distribution. Generally only hydrogen protons in the fluid will polarize. Those hydrogen protons in the matrix are too tightly bound to polarize, and when a sample is fully saturated with water, the generated signal amplitude can be calibrated to give the total porosity without knowing

matrix properties or mineralogy. On average, about 30 component T_2 distributions are generally combined to produce the histogram or cumulative pore-size distribution curve

Measurements made using a low-field NMR provide information on rock porosity, pore-size distributions, and in some cases, fluid types and saturations (Timur, 1967; Kenyon et al., 1986; Straley et al., 1994; Brown, 2001; Jackson, 2001; Kleinberg, 2001; Hurlimann et al., 2002). In this work, porosity, pore-size distribution and permeability estimates are the objectives for performing the NMR tests.

Although there are different NMR relaxometers available in the market place for laboratory analyses, Oxford instrument with 2MHZ magnetic frequency was used for this work, courtesy of Core Laboratories, ATC, Houston Texas (Figure 3-2).

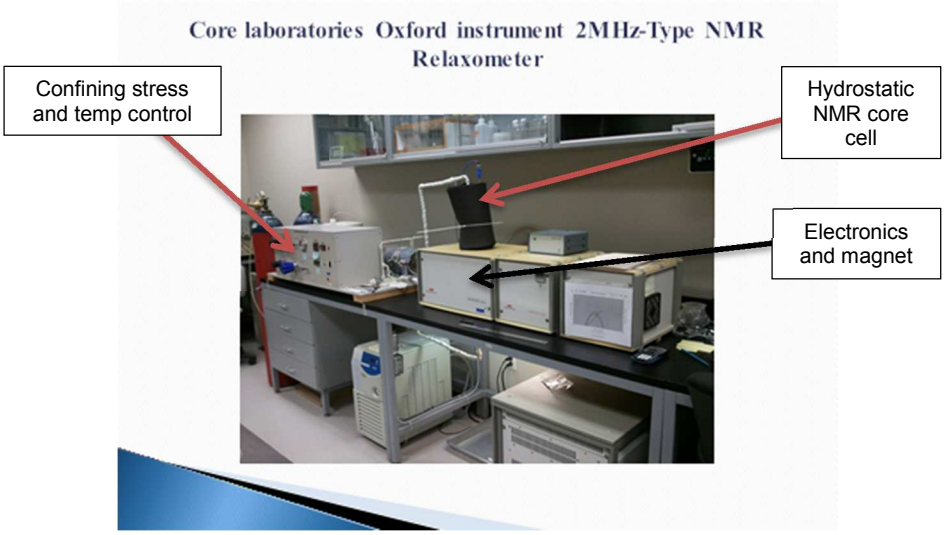

Figure 3-2: NMR Relaxometry setup.

3.2.1 Procedure for NMR Analyses:

A fully water-saturated sample was placed in a pre-weighed vial and cap, and weighed before being emplaced in the NMR relaxometer cell. In the relaxometer, a permanent magnet is applied to the sample to polarize hydrogen protons in the sample, generating

B_0, which is equivalent to T_1. A radio frequency pulse (oscillating magnet) is then applied to transversely align the protons, and the time it takes for transversely-aligned protons to align back to B_0 direction (longitudinally) is recorded. The DECAY, as is called, is exponential and goes from MAXIMUM (when the pulse is immediately removed) to MINIMUM (when the protons are fully aligned back to B_0 position). Spin echoes are collected and averaged during several scanning for calculations.

The experiments were conducted under the following conditions:

Hydrogen index = 1

Echo spacing (TE) (ms) = 0.20

Signal/noise (sat) = 200

Gradient = none

Temperature (^{0}C) = 28.0

The NMR pore volume ($V_{NMRpore}$) was calculated from the NMR experiments following equation 3-4:

$V_{NMRpore}$ = (Amp*Calib)/(NS*RG) ..... (3-4)

Where:

Amp = NMR amplitude after data inversion by Windxp

Calib = calibration factor to convert machine units to engineering units

NS = number of scans

RG = relative gain of the NMR relaxometer

NMR Derived Total Porosity (Phi_{NMR}) can then be calculated using equation 3-5:

$Phi_{NMR} = V_{NMRpore}/V_b$ ..... (3-5)

Where: $V_{NMRpore}$ = NMR calculated pore volume (mL)

V_b = bulk volume as calculated from routine rock properties (cm^3)

3.2.2 Permeability estimation from NMR test:

According to Core Laboratories' internal documents, three models are available for predicting permeability from NMR: Coates model, Mean T_2 Model (SDR Model), and Modified Coates model. Both Coates and modified Coates methods require NMR BVI and FFI information from de-saturated samples and were not applicable to this work.

Schlumberger Doll Research (SDR) Mean T_2 model was used for permeability estimation with equation 3.6 below

$$KT_{2LM} = (C*T_2logmean*Phi^2)^2 \quad \text{..... (3-6)}$$

Where:

KT_{2LM} = mean T_2 model NMR permeability (μs)

C = Empirical constant that depends on lithology (dimensionless). The value of C for this work was derived from the slope of air permeability and product of T_2 log mean and porosity squared.

Phi = NMR effective porosity (fraction)

3.3 Principles of Micro Ct Scanning:

Also called X-ray micro-tomography, CT scanning utilizes a class of scanner that can rapidly capture a series of scans at high resolution, which are reconstructed using a software to create a 3D model of the object scanned. The high resolution of CT allows individual grains and pores to be observed, and some conclusions drawn on their sizes and shapes. Its principle is based on Beer Lambert's law of light absorption and attenuation.

"Tomos" is the Greek word for "cut" or "section", and tomography is a technique for digitally cutting a specimen open using X-rays to reveal its interior details. A CT image is typically called a slice, and a slice corresponds to a certain thickness of the object being scanned. Where a typical digital image is composed of pixels (picture elements), a CT slice image is composed of voxels (volume elements).

One of the primary objectives of analyzing 3D scan images of reservoir rock is to perform pore network modeling or analyze the pore structure to determine its hydraulic properties. Pore network modeling is also one of the primary means to simulate hydraulic behavior of porous media at micro-scale levels (Rabbani A. 2014).

In this work, three sandstone samples were tested for Micro Ct Scanning, and their 2D data were processed using a software to obtain the pore characteristics and pore network information. Since a valid pore-scale analysis relies heavily on the accuracy of the pore identification and representation gained from image analysis, threshold reflecting porosity values corresponding to routine property figures were selected.

3.3.1 Procedure for Micro CT Scanning:

Three sandstones samples (Boise, Parker and Bandera Gray) were micro-CT scanned to generate 2D image slices. These three samples represent a wide distribution of basic

properties of porosity and permeability (Table 2-1). The 2D images were reconstructed into 3D and then analyzed for their pore structure properties using Avizo Fire software (Version 9.0, courtesy of FEI Visualization Sciences Group , Houston TX).

Courtesy of Core Laboratories, Houston Advanced Technology Center, these three sandstone samples were scanned at an average of 1.5 × 1.5 × 1.5 μm voxels, generating 1000 slices per sample. Porosity, pore size distribution, average pores sizes and throats were enumerated from these scans with Avizo.

In the image acquisition process, the 5mm × 5mm sample was placed in the path of an X-ray tube, and the image was captured on the digital detector as depicted in Figure 3.3 below. The X-ray shadow image corresponds to a two-dimensional projection from the three-dimensional object.

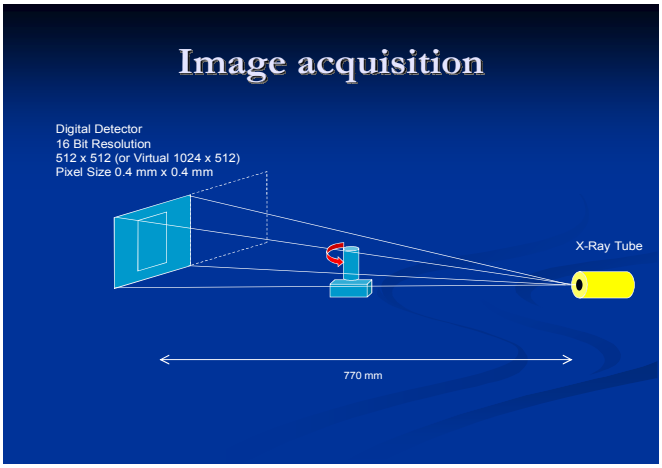

Figure 3-3: Typical image acquisition process

3.3.2 Processing:

In the processing stage, all 1000 slices for each sample was loaded into memory of the software and specific image slice was selected for processing reference. The image was loaded as gray scale image with a lattice information of 1000 × 1000 × 1000, uniform

coordinates. During image processing, a median filter was applied to the gray scale image for smoothing and denoising. Median filter is a smoothing module in Avizo software that uses a low-pass filter to reduce contrast and soften edges of images (Avizo 9.0 User's Guide).

3.3.3 Image segmentation:

Sample segmentation allows a separation of the pores from the matrix and enumeration of the pores for computing total pore volume and porosity.

Binarization is a module under image segmentation that allows the transformation of a gray level image to a binary image (Figure 3-4).

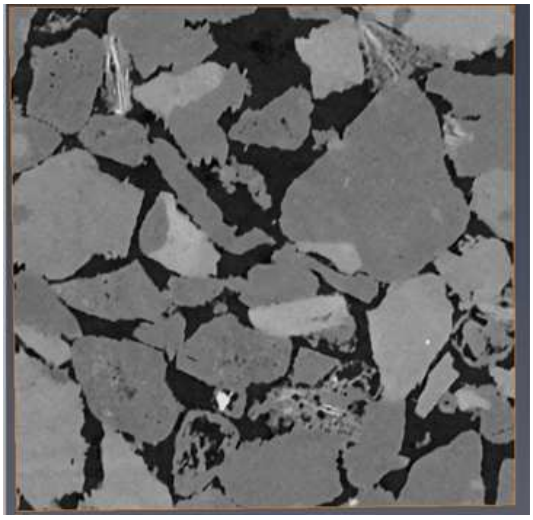

Figure 3-4: Gray level image of Boise with a default color map of 1709-50960

This method is used when the relevant information in the gray level image correspond to a specific gray level interval. Interactive thresholding is one of the options of binarization, and was applied to the image to isolate the matrix from the pores. The output is a binary image that gives a high intensity value to target segment of image and lower intensity number to the other. Several thresholding tools available in Avizo software for processing were tested during segmentation, but most of them led to wrong

conclusion. For example, using “Auto Thresholding” isolates the grains instead of the pores and does not provide option to change (Figure 3-5).

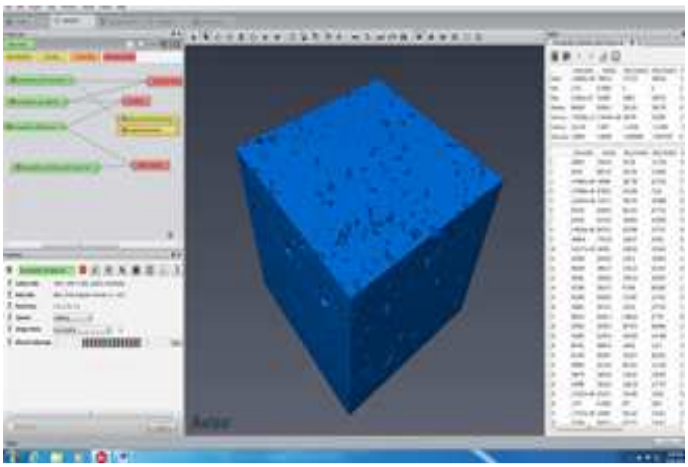

Figure 3-5: Isolation of grains instead of pores using Auto Threshold HIGH

“Interactive thresholding”, on the other hand, also gave a priority to matrix instead of pores, but option was available to reverse it by altering the Color Map and Intensity Range (see Figures 3-6 and 3-7).

In Figure 3-6, Color Map was 1941-48608 and Intensity Range 5039-48608 by default and matrix has a higher intensity. However, by changing Color Map to 2327-4900 and Intensity Range to 10-4800, Figure 3-7 was generated, which is the reverse of Figure 3-6. The implication is that if the focus was not changed, all enumeration, labeling and label analysis will be performed on the grains or matrix rather than the pores.

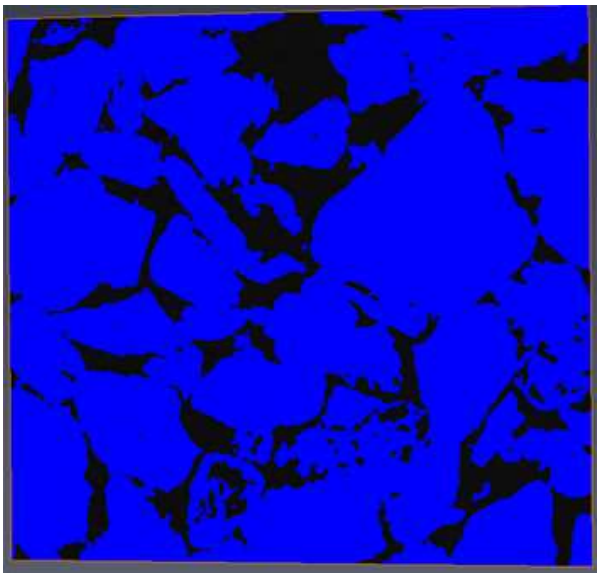

Figure 3-6: Interactive thresholding with the matrix (in blue) having higher intensity than the pores (in black).

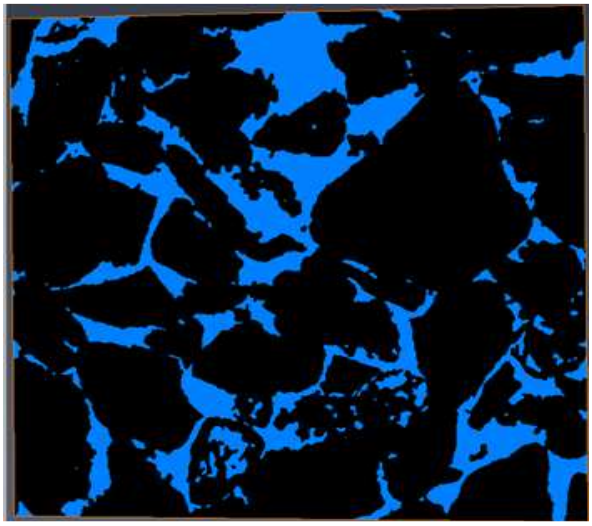

Figure 3-7: Interactive thresholding with the pores (in blue) having higher intensity than the matrix (in black)

3.3.4 Image Separation:

Image separation is a module under image processing, and one of the tools it uses is called “binseparate”. Binseparate computes the watershed of an image, and it helps to further identify connection lines between pores and separate them along those lines.

“Binseparate” can be applied in five different modes in the Avizo software. Only two of the modes were applied on our samples in this work. The first is called “binseparate with connected objects” (watersheds without separation lines masked by the binary input image), which allows for a generation of pore network model with throats, and requires no labeling. The second is called “binseparate with splits” (original data minus separation lines), which allows for labeling, label analysis and generation of pore network models without throats (Figure 3-8). Both methods were applied to each sample to compare and confirm the results.

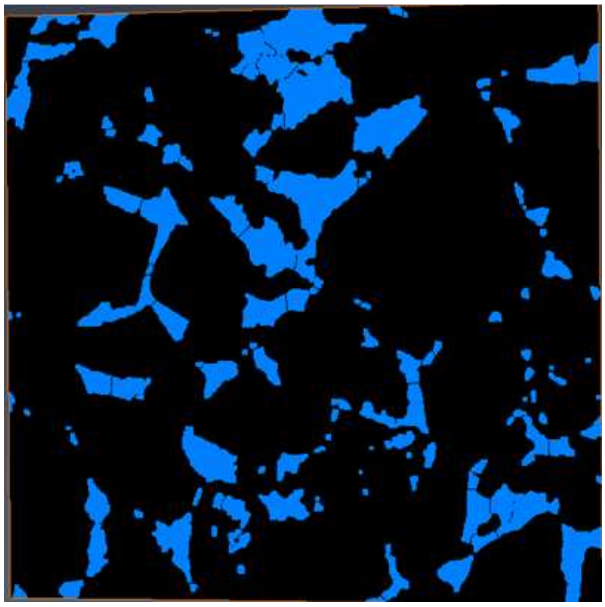

Figure 3-8: Output of “binseparate with splits” tool on Boise sample

Volume fraction (the proportion of image occupied by pores) analysis for porosity estimation can be applied to binary or labeled images. In this work, volume fraction was applied to interactive thresholded images (binary images) to estimate porosity. It was run in two modes: the first was 3D to provide an overall volume fraction of the 3D object (Figure 3-9), and the second was XY plane and volume fraction provided on a slice-by-slice basis.

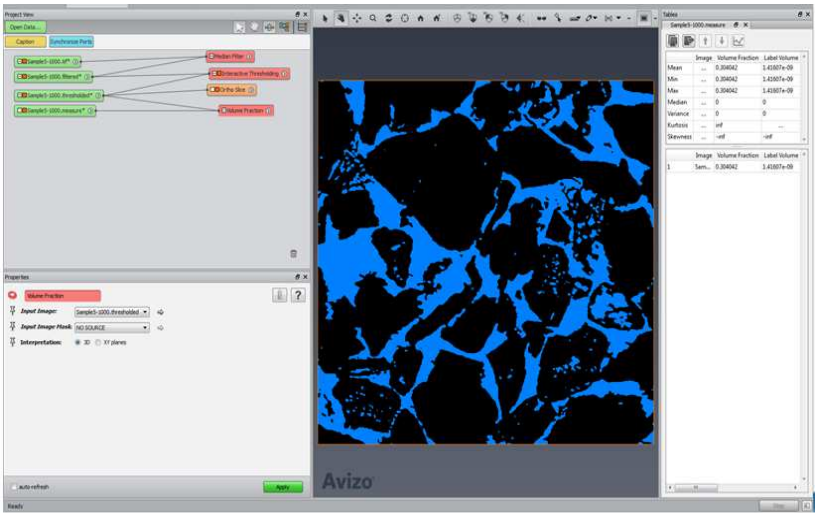

Figure 3-9: Output of “3D volume fraction” to compute total porosity

After using “binseparate with splits” on the image to further separate the pores, another tool called “label” was applied to the image to enumerate the pores with eight separate colors that are repeatable (Figure 3-10).

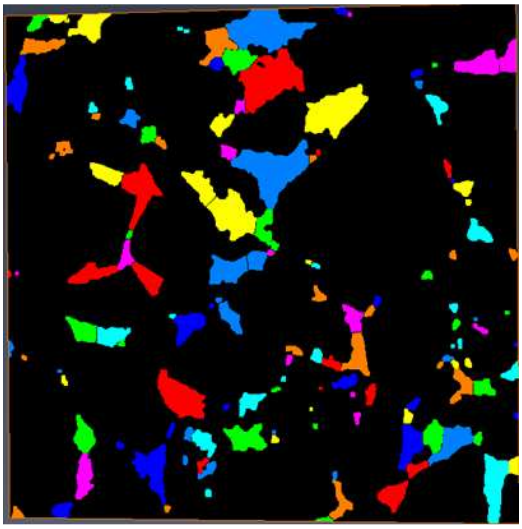

Figure 3-10: Output of “label” tool on Boise sandstone

“Label tool” performs connectivity analyses of individual objects in the entire 3D volume. Each pixel in an individual object is assigned with an identical value, and each object is assigned a different consecutive value, starting from value 1 through 9; the color

assignment is then repeated. The maximum value gives the total number of objects in the original binary image.

After enumeration using “label tool”, another tool called “I_Analyze” (or interactive analyzer) was applied to the separated image to provide details regarding the pores. The “label analysis” command computes a group of measures on each cell or connected component of the input image, and generates a spreadsheet with the result values. Results are generally expressed as the coordinate unit on the original image (microns). Although “label analysis” only requires input label image or binary image, but applying intensity image as an option allows the computation of data statistics like histogram.

“Label analysis” can be run in two modes. First was “basic label analysis”, in which volume, area and directional properties of each enumerated pores are provided for each slice (Figure 3-11). The second mode “diameter label analysis” was a modified procedure focused on equivalent diameter and sphericity of the pores. Other parameters like hydraulic radius, can be added if appropriate equations are known (Figure 3-12). In this work, both modes were run on the samples.

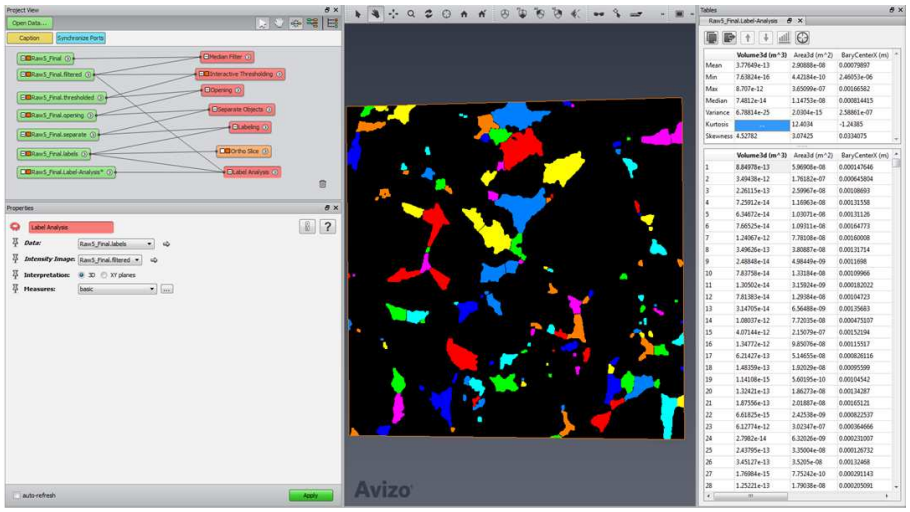

Figure 3-11: Output of “basic label analysis” on Boise sandstone

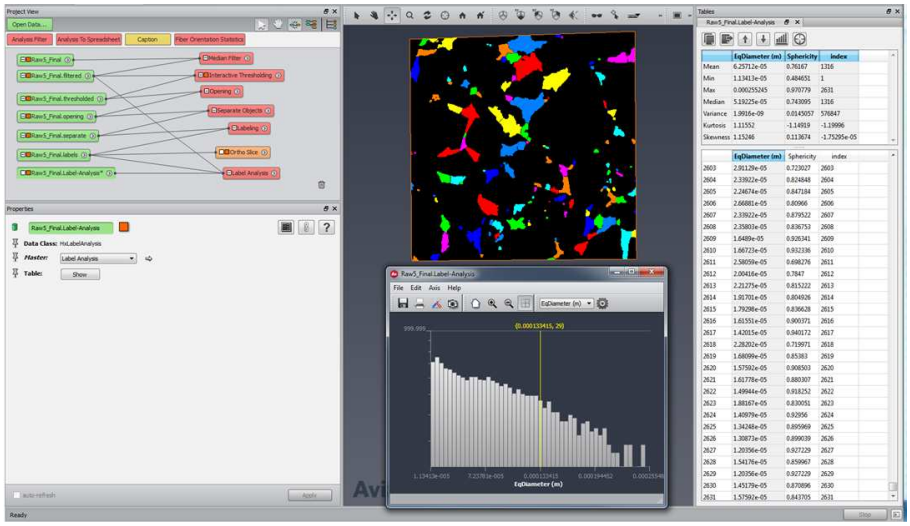

Figure 3-12: Output of “diameter label analysis” on Boise sandstone with histogram.

At the end of this analysis, “binseparate with splits” was deleted and “binseparate with connected objects” was run on the sample to Generate Pore Network modules with throats (Figure 3-13).

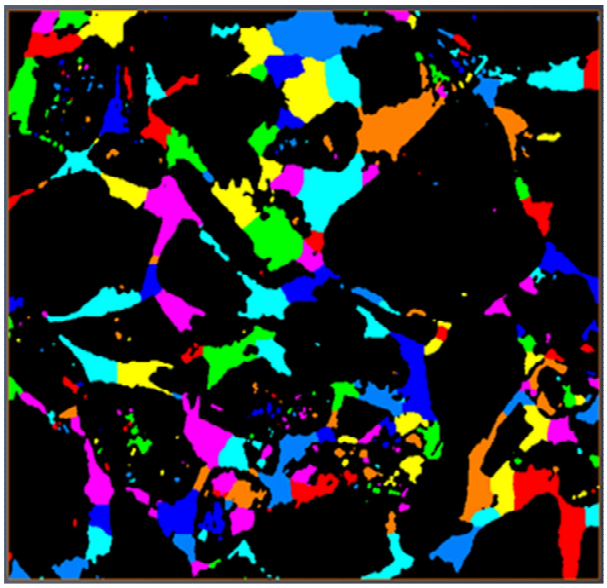

Figure 3-13: Output of “binseparate with connected objects” tool on Boise sandstone

“Generate Pore Network Modules” were run on the separated images to generate pores, throats and coordination numbers for each sample. “Generate Pore Network Module” takes a labeled image representing the pore space and output the corresponding pore network model. The extracted network contains a number of nodes, a number of throats, coordination number, throat equivalent radius, throat channel length (defined as distance from pore to pore center), pore equivalent radius and pore volume (Figure 3-14).

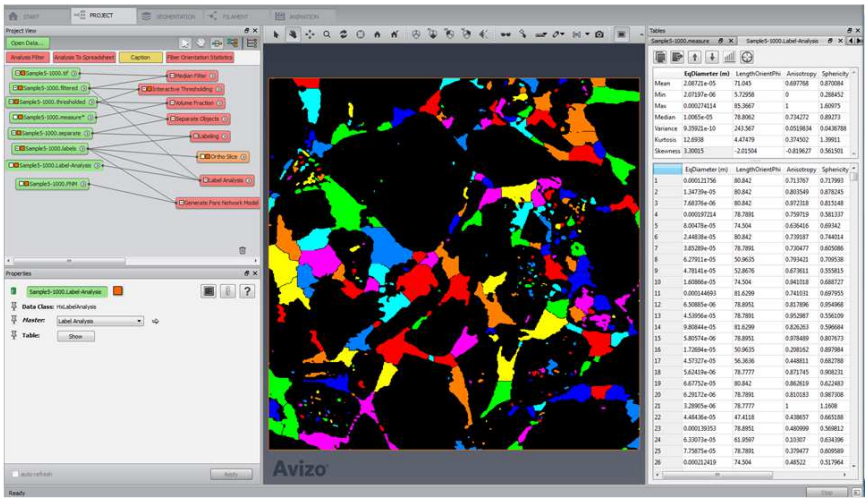

Figure 3-14: Output of “pore network model” on Boise sandstone (compare Figure 3-11)

The generated data are too large to be included in this thesis, but a statistical summary of each data is presented in the section of Results and Discussion. Permeability using Stokes Law was not computed because of equipment limitation, as our available computer does not have an adequate memory and CPU power to complete the computation.

3.4 Principles of Fluid Imbibition:

Imbibition is described as the intake of a wetting phase into pore spaces of a porous media by capillary forces (Buckley, 2001; Abe, 2005; Hu et al., 2012). Two types of imbibition processes are common: (1) forced imbibition, where an external force is applied to promote displacement of fluid, and (2) spontaneous imbibition, where fluid penetrates the capillary media due solely to the potential generated by wettability difference at the solid wall with respect to the contacting fluid (Lopez and Soria, 2007).

Spontaneous imbibition is a capillary dominated process and the imbibition rate depends on properties of the porous media, the fluid involved, and the fluid rock interaction. Although fluid imbibition in oil and gas reservoir studies can be used as an indicator of wettability, critical gas saturation and/or pore connectivity, it was used as pore connectivity indicator for this work.

Fluid imbibition is a simple procedure that allows observation and determination of rock's pore connectivity. The test involves exposing one face of the rock sample to water or an organic fluid and measuring the mass of water or fluid uptake over time via a recorded increase of sample weight. The concept is mathematically analogous to diffusion in that, in classical homogenous materials and if gravitational effects are negligible, the distance (l) to the wetting front increases with the square root of time according to Bruce and Klute (1956) and Philip (1957).

This study focuses on spontaneous imbibition of seven sandstone samples using de-ionized (DI) water, to observe how this fluid move through pore spaces and, act as a quick way to probe the pore connectivity of the samples. Using network modeling results of Ewing and Horton (2002) which is based on percolation theory, we are able to estimate pore connectivity as indicated by the slope of log imbibed liquid mass versus log time. If the accessible porosity is uniform with distance or there is adequate pore connectivity,

then the cumulative mass of imbibed water “I” behaves identically. This gives a slope value of 0.5 in log scale. A slope of ~0.25 indicates that pore connectivity is barely above the percolation threshold, and it follows that below this threshold, connected pores do not exist across the study domain. This can be compared to high coordination numbers for the same sample in the enumeration of pores obtained from micro CT scans test.

3.4.1 Procedure for Fluid Imbibition:

In the spontaneous imbibition experiment, each sample was run four times, with the $1cm^3$ cube sample having triplicate measurements and one measurement on the cylinder plug. All fourteen sandstone samples (cube and cylinder for each of seven sandstones) were oven-dried at 60°C for at least 48 hours before being subjected to the imbibition experiments. In addition, the $1cm^3$ cube samples were dried in 60°C oven for at least 8 hours to ensure a constant weight between triplicate runs. Several weights were taken for each sample to be certain that a constant weight is achieved before imbibition experiment, and samples were placed in a desiccator to cool to ambient temperature before each weighing.

All fourteen samples used in the experiment have all sides, except top and bottom, coated with quick-cure transparent epoxy to allow one-dimensional imbibition and avoid evaporation of the imbibing fluid through the side surfaces of the samples. The imbibition setup as shown in Figure 3-15 was used for the experiment.

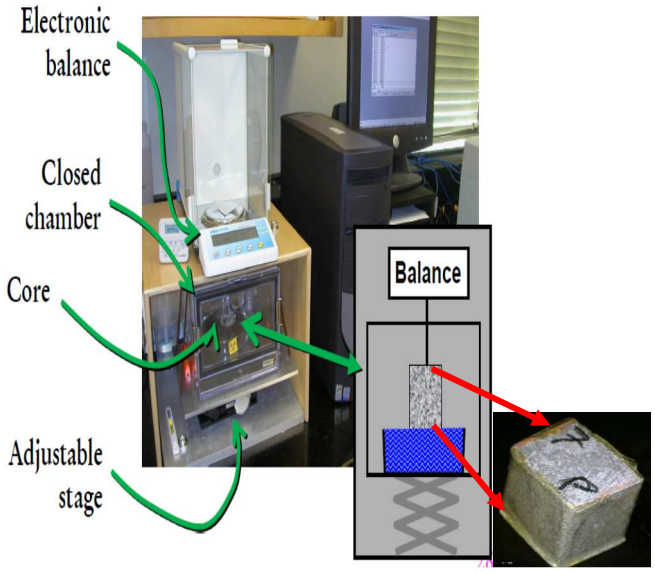

Figure 3-15: Setup for the fluid imbibition

During imbibition tests with de-ionized water, separate beakers of water was placed inside the experiment chamber to maintain a constant, and high, relative humidity inside. The top-side of the epoxied sample was clamped and the bottom-face lowered to touch a petri dish containing imbibition fluid (DI water in this work) in the chamber. The imbibition rate was monitored by automatically recording the sample weight change over time, using a bottom-weighing (for hanging the rock sample) analytical balance with a resolution of 0.1 mg (Shimadzu Analytical Balance AUW220D). A final dry weight of the sample was taken immediately before clamping and allowing to begin water imbibition.

Three imbibition test run-times for the 1 cm-cube sample were 10, 30, and 60 minutes, respectively. The cylinder-plug sample was mostly ran for about 5 hours, except for Crab Orchard that ran for twelve hours and Idaho Gray that was ran for one hour because of their extremely low and high permeabilities.

Chapter 4

RESULTS AND DISCUSSION

4.1 Mercury Injection Capillary Pressure (MICP):

During data processing, intrusion pressures are directly converted to corresponding pore throats radius using the Washburn equation below

$$\mathrm{Ri} = (2\gamma * \cos\theta * \mathrm{C})/\mathrm{Pc} \quad \text{..... (4.1)}$$

Where Ri = pore entry radius (microns)

$\gamma = \text{interfacial tension } (\frac{\text{dynes}}{\text{cm}})$

Θ = contact angle (140 degrees)

C = Washburn conversion constant (0.145, to obtain microns)

P_c = mercury injection pressure (psia)

Table 4-1 below shows details of the summary of data for MICP experiments. In addition, three plots are generated. The first plot which is cumulative and incremental intruded pore space as a fraction of mercury occupied pore volume is plotted against pore throat sizes as distribution curves. This semi-logarithmic curves represent pore-throat distribution curves for the samples. Typical plots for Boise sandstone is presented in Figure 4.1. The incremental plots also provide the dominant throat within the sample that controls permeability. The second plot is the pore size distribution histogram, which shows pore-throat radius against mercury saturation frequency, by displaying a range of pores and their frequency of occurrence in the sample (Figure 4.2). Finally a plot of typical drainage and imbibition showing mercury intrusion and extrusion against intrusion pressure is displayed (Figure 4.3). This plot is particularly important for reservoir completion, wettability examination and reservoir completion. It is generally used to determine irreducible water saturation.

Table 4-1: MICP result for all samples

Mercury injection Data Summary												
Sample ID	Bulk density at 0.58 psia (g/cm^3)	Apparent skeletal density (g/cm^3)	R_{50} median pore throat (μm)	Approx. pore -throat threshold (μm)	Dominant pore throat size (μm)	Total pore area (mL/g)	Median pore radius (vol) (nm)	Median pore radius (area) (nm)	Average pore radius (nm)	Swanson perm (mD)	Porosity (fraction	Entry pressure pd (psia)
Idaho Gray	1.748	2.598	49.3	105	50	39.8	49317	5.7	159.4	13700	0.327	<1
Boise	1.839	2.605	21.9	120	25	41.1	22146	8.8	131.24	2740	0.29	2.5
Gray Berea	2.109	2.637	6.02	15	10	29.1	6860	21.8	103.6	150.74	0.2	10
Bandera Gray	2.143	2.676	1.91	8.02	2.5-5	56.4	1348	4.4	43	21.6	0.2	25
Parker)	2.177	2.653	2.34	9.03	2.5- 5	22.2	1246	16.7	103.5	26.3	0.179	20
Kentucky	2.288	2.672	0.47	1.32	0.75	38.1	376	12.4	60.7	1.22	0.144	100
Crab Orchard	2.461	2.649	0.118	0.55	0.25	43.9	125	5.4	28.6	0.0345	0.071	500

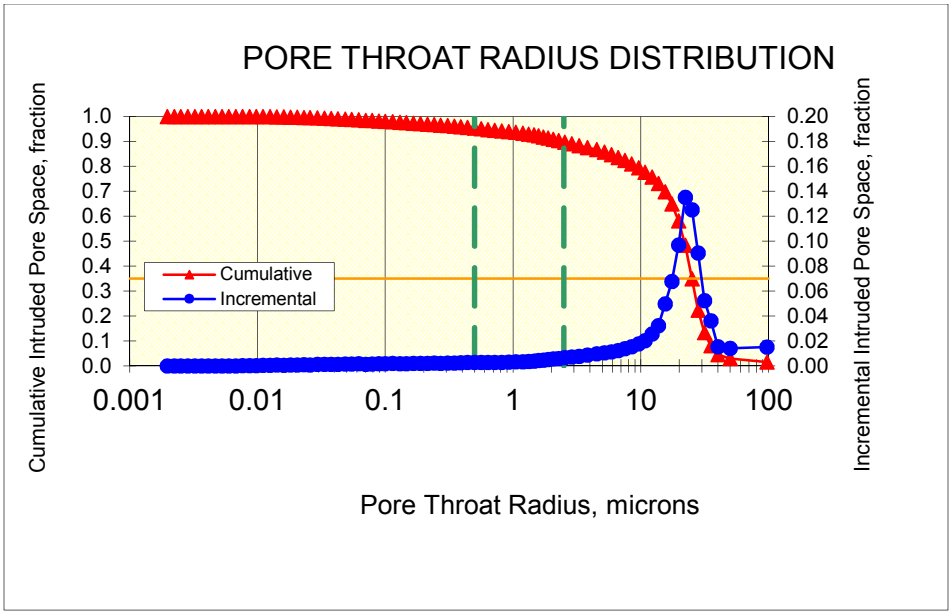

Figure 4-1: Pore throat distribution for Boise sandstone

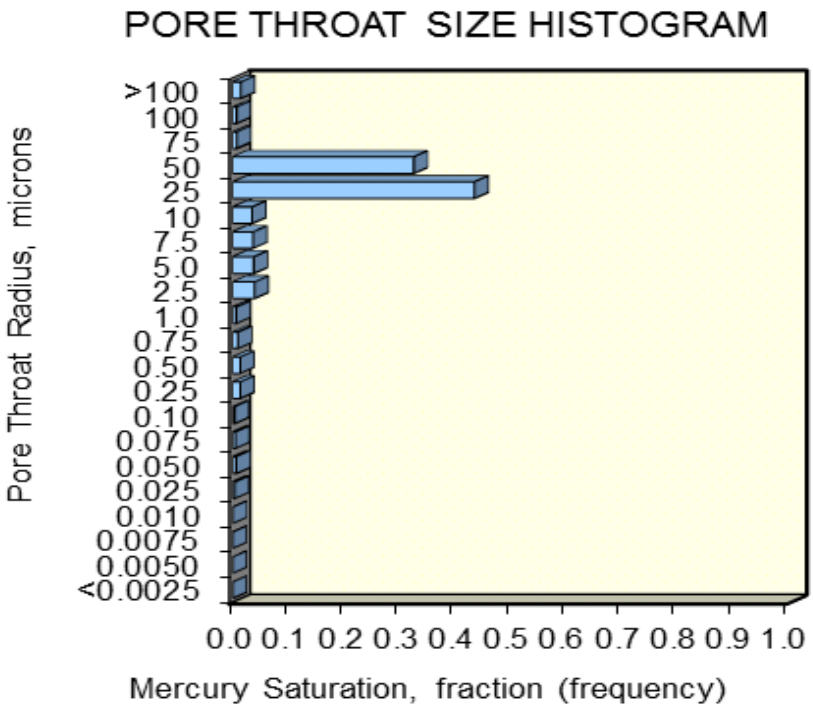

Figure 4-2: Pore throat histogram for Boise sandstone

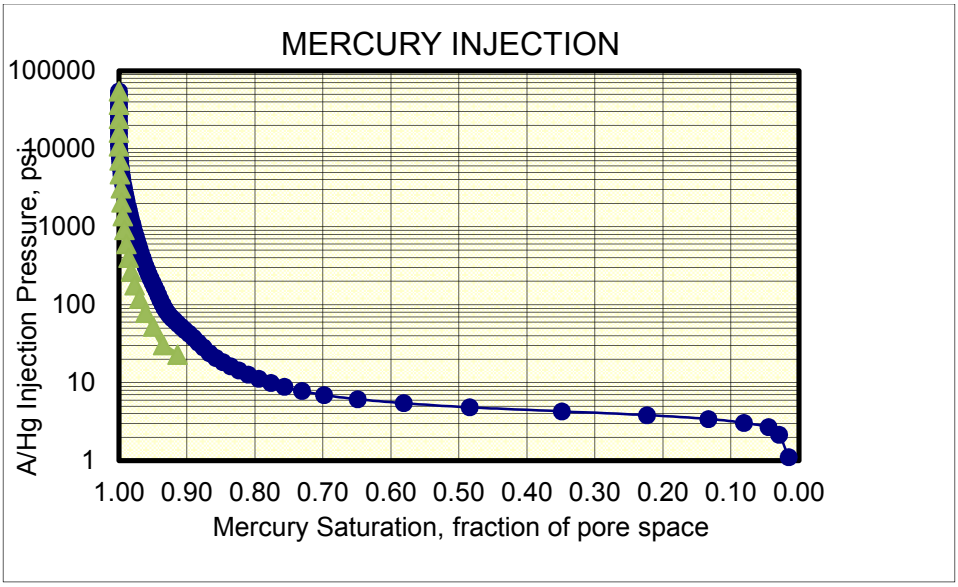

Figure 4-3: Capillary pressure curve for Boise sandstone

Result of the test shows the samples having a wide range of throat peaks that could be correlated to their respective permeability. The throat peak range from close to 100 µm on the high end of the fifth log cycle for Idaho Gray, to 0.08-0.2 µm for Crab Orchard. Results not shown in report

Median pore throat (R_{50}) is generally used for permeability estimation. On these sample-set it follows the same trend of dominant peaks. It ranges from 49.3 µm for Idaho Gray to 0.118 µm for Crab Orchard. Accordingly, Swanson permeability too ranged from 13700 md for Idaho Gray down to 0.0348 md for Crab Orchard.

Mercury entry pressure (p_d) is the initial pressure required to intrude the largest pore. It can be correlated to permeability in an inverse relationship. Larger pore-throats and connectivity shows lower entry pressure and thus may lead to a higher permeability. This is clearly demonstrated in the capillary curves for different samples. For example, Idaho Gray has highest dominant pore throats with a range of 50-100 µm and has the

lowest entry pressure (p_d). This translates to Idaho Gray having the largest permeability. The same trend is observed on all of seven samples. A little departure is observed in Bandera Gray and Parker. Although Bandera Gray and Parker both has 2.5-5 μm dominant pore-throats, the availability of 7.5 μm throats in Parker led to its higher Swanson permeability. This is also reflected in lower entry pressure of mercury injection for Parker compared to Bandera Gray.

From this suite of sandstone samples, and especially suited for clastics, entry pressure could be correlated to pore sizes in terms of whether macro, meso or micro categories. Entry pressure less than 10 psia correlates to macro pores, while 10-25 psia trends borderline between meso and macro pores, and 25-100 psia falls into meso and finally any pressure over 100 psia trend micro pores.

Another observation is that because the throats are larger and the pore bodies are readily connected leading to better fluid flow, the imbibition plot shown through mercury extrusion is more parallel to drainage plots, meaning less trappings of mercury in the pores when the pressure is lowered (less hysteresis behavior) (Figure 4-3). As the entry pressure goes higher, meaning smaller throats, a snap-off or ink-bottle phenomenon may be experienced, where part of the mercury will be trapped in the pores after pressure is lowered.

Apart from porosity and permeability values, other petrophysical parameters such as bulk density, apparent density, R_{35}, R_{50} and dominant pore throat values are shown in Table 4-1.

In terms of pore size distribution, all the samples tested for mercury intrusion displayed a single peak of dominant pore or mono-modal types with dominant pore size ranging from 50 μm to 0.25 μm. The value of the dominant pore throat size also correlates well with permeability.

Porosity results from mercury injection in these samples compare well with porosity from helium and other tests as indicated in Table 4-11 below under porosity discussion.

4.2 Hydrogen Proton Nuclear Magnetic Resonance (NMR):

Proton NMR measurements were made on all the samples at 100% brine saturation using an Oxford Instrument type core analyzer operating at 28°C and approximately 2MHz T_2 measurements were made in a homogeneous magnetic field using the CPMG method with phase alternation and an inter-echo spacing TE=0.2 msec. A sufficient number of echo trains were measured and stacked to achieve a minimum signal-to-noise ratio of 200:1. Table 4-2 below show details of data from the test.

For the samples that are fully saturated with brine, the rate of decay of the NMR signal is described by a distribution of decay times called transverse relaxation times (T_{2s}), with the general equation described in equation 3-3 above. The resulting NMR signal is a composite of all the NMR signals from the different pore sizes in the core, and a mathematical procedure known as inversion is used to process the composite NMR signal and separate it into its component parts as indicated in Figure 4-5.

The result of the inversion process is a T_2 distribution showing the relative population of the individual T_2 decay times that make up the composite NMR signal from the core. Example is the T_2 distribution curve for Boise sandstone shown in Figure 4-4, with dominant pores in the range of 80–1000 ms (macro pores).

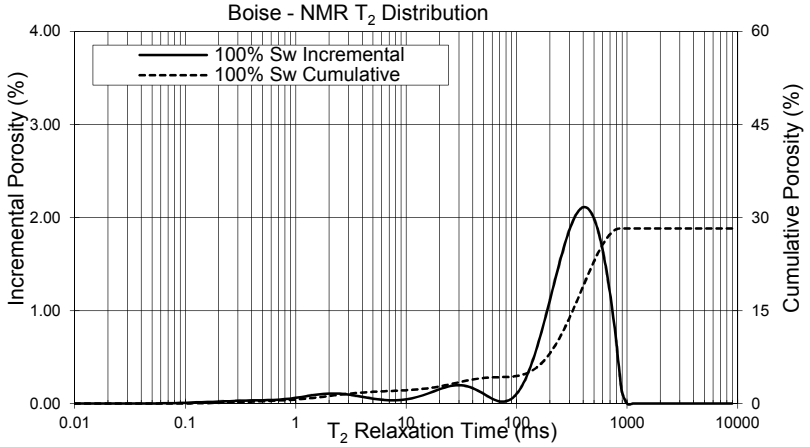

Figure 4-4: NMR T_2 distribution for Boise sandstone

Because long T_{2s} come from large pores and short T_{2s} from small pores, this T_2 distribution is in effect a model of the pore size distribution in the core. An area under the T_2 curve represents the total porosity. This porosity is independent of the lithology of the rock matrix.

T_2 within 2.8 ms or less is the shortest T_2 time and is said to represent clay bound water. It is subtracted from total porosity to give effective porosity according to Corelab internal document.

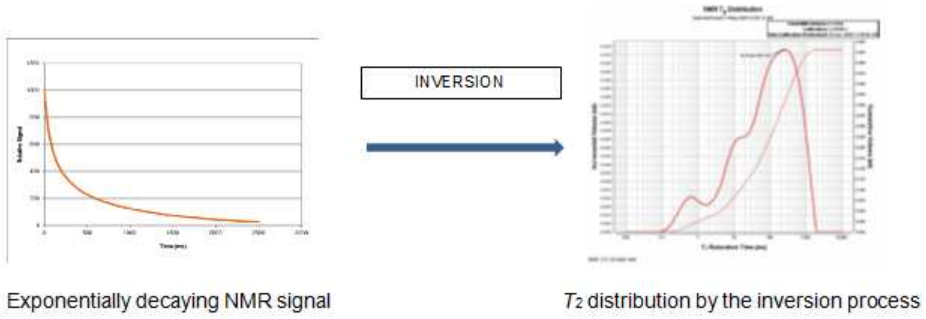

Figure 4-5: Transformation of NMR decay signal to T_2 distribution through INVERSION process

The data from all samples show a wide range of dominant T_2 times corresponding to high and low permeability like the mercury injection tests. They range from 80-1000 ms for Idaho Gray down to Kentucky with a maximum peak at 100 ms.

A detail of the dominant peaks is listed in Table 4.3 below. As shown in the T_2 distribution plots of all the samples, the larger the dominant pore sizes the longest the T_2 time. Hence higher permeability samples have the longest T_2 time and low permeability samples have lowest T_2 (Talabi et al., 2009). A departure from that trend can be seen between Crab Orchard and Kentucky sandstones. Crab Orchard clearly shows a larger T_2 but smaller permeability. The porosity or pore space of Kentucky sandstone doubles that of Crab Orchard sandstone. Hence in correlating T_2 with permeability, correlation

between porosity and permeability should be considered too especially in clastics where the correlation is generally acceptable.

Table 4-2 below also shows the direct relationship between T_2 time and NMR permeability. The difference between total NMR porosity and effective NMR porosity is the clay bound water as indicated in Table 4-2 below and it represent the shortest T_2 time.

Table 4-2: Generated NMR data sorted from the highest T_2 to lowest

	Core Analysis Data		NMR Data				
			100% Brine Saturation				
Sample name	NCS (psi)	Porosity (%)	Porosity (%)	Effective porosity (%)	Clay Bound Water, (T_2 max = 2.8 ms)	T_2 Log Mean (ms)	Perm using T_2 Log Mean model
Idaho Gray	800	32.8	33.6	32.4	1.2	406.4	46141.2
Boise	800	28.5	28.3	26.7	1.6	191.5	4724.8
Gray Berea	800	20.1	19.5	18.4	1.1	86.9	219.4
Bandera Gray	800	19.9	19.5	17.2	2.3	28	17.4
Parker	800	18.1	18	15.3	2.7	25.8	9.2
Crab Orchard	800	7.3	7.2	6	1.2	12.5	0.1
Kentucky	800	14.4	15	11.8	3.2	8.6	0.4

Table 4-3: Pore size classification and interpretation

Sample name	NMR Data			
	100% Brine Saturation			
	Macro Pores (ms)	Meso Pores (ms)	Micro Pores (ms)	Interpretation
Idaho Gray	200 - 1500	8 - 50	0.2 - 5	Almost no transition between pores but very large dominant macro pore
Boise	80 - 800	8 - 70	0.2 - 7	Tiny transition between meso and micro pores
Gray Berea	30 - 600	2 - 20	0.2 - 2	Transition between pores
Bandera Gray	10 - 350	1 - 8	0.2 - 1	Very large transition between pores
Parker	15 - 500	1 - 15	0.2 - 1	Large transition between pores
Crab Orchard	A single peak trending 0.3 - 400ms with a peak at 10ms.			Could be classified as MESO
Kentucky	A single peak trending 0.2 - 100ms with a peak at 18ms.			Could be classified as MESO

4.2.1 Surface relaxivity:

Surface relaxivity is a measure of surface's ability to cause a proton to relax. Although hydrogen protons in the pores of a porous material relax in three mechanisms: bulk fluid, surface and diffusion in the presence of magnetic field gradient, the main relaxation mechanism for water in porous media is surface relaxation. It occurs at the fluid-solid interface where the hydrogen protons approach grain surfaces and transfer energy to the walls.

Relationship between T_2 relaxation, surface to volume ratio and surface relaxivity is aptly described in equation 3-3. The relationship implies that protons in smaller pores will relax faster than those in larger pores since smaller pores have larger surface-to-volume ratio which enhances surface relaxation rate ($1/T_{2s}$). So the larger the pores, the smaller the surface-to-volume ratio.

Surface relaxivity differs with rock types and it is generally higher for clastics than carbonates. They are independent of temperature and pressure. In general surface relaxation falls between 0.003 – 0.03 cm/sec for clastics (Schon J.H., physical properties of rocks: A workbook)

Because the T_2 decay rates can be related to surface-to-volume ratio or internal pore surface (pore size), three general rules are derived (Schon J.H., Physical properties of Rocks: Workbook). The first one is that short T_2 are associated with small pores, large surface-to-volume ratio, and low permeability. The second one is the opposite. Long T_2 indicates large pores, small surface-to-volume ratio and high permeability. Finally the shortest T_2 can be correlated to clay bound water and hence use as CEC indicator, and also used to differentiate between total and effective porosity.

4.2.2 Permeability estimation using NMR data:

The Schlumberger-Doll Research (SDR) permeability equation was used in this project according to equation 3-6.

The SDR equation assume that a good correlation exists between porosity, pore-body and pore-throat size, and pore connectivity. This assumption is generally valid in clastic (e.g., sand/shale) sequences, but in carbonates or other lithologies, this model and others like it may not be reliable

The constant "C" value of 5.035 from our dataset was derived from the slope of air permeability and the product of square of total NMR porosity and T_2 Log mean. Note that Idaho Gray permeability was excluded in the slope determination. As seen in Table 4-5 below, permeability using SDR compares favorably with permeability from other sources.

Table 4-4 Summary of permeability values from all approaches

Sample name	Permeability (mD)			
	Air Perm	API Brine Perm	SDR Perm	Swanson Perm
Idaho Gray	>50 Darcy	22100	46141.2	13700
Boise	4780	5400	4724.8	2740
Gray Berea	176	104	219.4	150.74
Bandera Gray	20.7	12.9	17.4	21.6
Parker	19.5	9.60	9.2	26.3
Kentucky	0.608	0.149	0.4	1.22
Crab Orchard	0.026	0.00337	0.1	0.0345

4.3 Micro Computer Tomography scanning (micro Ct Scan):

3D processing of micro Ct scans provides valuable information that aids in pore structure characterization. Equivalent pore diameter and pore throats provide a direct input into pore size distribution when plotted against their frequency or volume percentages. Table 4-5 below provides a detailed summary of the data generated.

Because of large data output for each sample, details of the data could not be presented in the thesis, however, a statistical summary of all data generated from sample processing is provided below in Tables 4-6 and 4-7 below

Table 4-5 Original data as generated from processing. It includes the zero diameter pores.

Sample name	Bandera Gray	Parker	Boise
Sample dimension	1.5μ	1.5μ	1.67μ
number of voxels (tif voxels)	1000	1000	1000
3D Porosity (fraction) from Ct Scan	0.193	0.172	0.304
# of pores per sample using PNM (Pores with coordination # and throats) using separated image with connected objects	14386	14136	16250
# of throats per sample using PNM (Pores with coordination # and throats)	7247	5521	9162
# of pores per sample using PNM without throats derived from Label image only	14468	14199	16294
Total number of enumerated pores per sample using “Basic Label Analysis”	14468	14199	16294
Total number of enumerated pores per sample using “Diameter Label Analysis”	14468	14199	16294

Pore-body and pore-throat size distributions were plotted against their frequencies using equivalent diameter and throat data. Result is depicted in Figures 4-6 through 4-8.

From our sample analyses, the largest pore radius range from 137 to 94.2 μm. Average pore radius range from 10.6 μm for Boise to 7.66 μm for Parker. Largest throat

radius on the other hand ranges from 102 μm for Boise to 50.7 μm for Bandera Gray. Bandera Gray and Parker sandstones exhibit almost the same characteristics in terms of average pore and throat radius.

Boise sandstone produces a single or mono-modal distribution curve in the 0-25 μm. However, both Parker and Bandera Gray sandstones show a bi-modal behavior, with both of their dominant peaks located primarily at 0-15μm and secondarily at 20-70 μm.

4.3.1 Pore connectivity parameter:

Coordination number is a key pore connectivity parameter and it is defined as the number of entry and exits to a pore. In the three samples processed with CT Scans, Boise with the highest permeability also has the highest coordination number, with the highest of 39 and average of 4.47 (out of a net count of 4103).

At a net count of 2099, Bandera Gray has highest coordination number of 31 and average of 6.905. Parker has a net count of 1573, and the highest coordination number of 32 and average of 7.02. All of these coordination numbers indicate good connectivity for these sandstones, and the coordination number distribution is listed in Figures 4.7, 4.10 and 4.14 for these samples.

These are preliminary results, because the complimentary license of Avizo provided to UTA was only for a short period of six weeks. For all three sandstones, most of the pores have zero radius and zero coordination numbers and we are not sure whether it is from processing error or artifacts from the software, For example, out of a total of 16250 pores enumerated for Boise, 12147 pores have a zero coordination number and it is not suspected that such a large number of pores in permeable Boise sandstone are either closed or isolated pores. Similarly, out of a total of 14386 pores enumerated for Bandera Gray, only 2099 have a positive coordination number. Out of the

14136 pores enumerated for Parker, 12563 have zero coordination number. A total of 78 zero radii of 14136 pores enumerated for Parker was also removed and statistics re-calculated.

A total of 5521 throats were enumerated for Parker. The largest throat radius is 56.34μm and smallest is 0.363μm, with an average of 9.93μm and a median of 8.62μm. That information and details for Boise and Bandera Gray sandstones are listed in Table 4-9 below.

Table 4-6: CT scan statistical summary generated with Avizo software.

STATISTICAL INFORMATION ON SAMPLES							
Coordination number Statistics				Porosity statistics (XY Slices for 1000 slices)			
	BANDERA GRAY	PARKER	BOISE	*Fraction	BANDERA GRAY	PARKER	BOISE
Mean	1.01	0.78	1.13	Mean*	0.193	0.172	0.304
Min				Min*	0.170	0.143	0.243
Max	31.00	32.00	39.00	Max*	0.209	0.208	0.383
Median	0.00	0.00	0.00	Median*	0.193	0.173	0.306
Variance	8.79	6.80	7.55	Variance	0.000	0.000	0.001
Kurtosis	15.15	19.92	21.03	Kurtosis	-0.639	-0.111	-0.818
Skewness	3.62	4.10	3.83	Skewness	-0.337	0.304	0.026
Pore Equivalent Radius Statistics				Pore Equivalent Diameter Statistics			
	BANDERA GRAY	PARKER	BOISE		BANDERA GRAY	PARKER	BOISE
Mean	8.84E-06	7.62E-06	1.05E-05	Mean	1.76E-05	1.52E-05	2.087E-05
Min	0.00E+00	0.00E+00	0.00E+00	Min	1.86E-06	1.86E-06	2.072E-06
Max	9.42E-05	1.23E-04	1.37E-04	Max	1.88E-04	2.45E-04	2.74E-04
Median	4.03E-06	3.58E-06	4.93E-06	Median	8.02E-06	7.16E-06	9.837E-06
Variance	1.68E-10	1.53E-10	2.39E-10	Variance	6.64E-10	6.04E-10	9.359E-10
Kurtosis	6.32E+00	9.70E+00	1.24E+01	Kurtosis	6.40E+00	9.80E+00	1.27E+01
Skewness	2.60E+00	3.10E+00	3.27E+00	Skewness	2.61E+00	3.11E+00	3.30E+00

Table 4-7: CT scan statistical summary generated with Avizo (continued)

STATISTICAL INFORMATION ON SAMPLES							
Throat Equivalent Radius Statistics				Pore Volume Statistics			
	BANDERA GRAY	PARKER	BOISE		BANDERA GRAY	PARKER	BOISE
Mean	9.69E-06	9.93E-06	1.63E-05	Mean	4.531E-14	4.1E-14	8.714E-14
Min	3.63E-07	3.63E-07	4.04E-07	Min	0	0	0
Max	5.07E-05	5.63E-05	1.02E-04	Max	3.504E-12	7.72E-12	1.088E-11
Median	8.50E-06	8.62E-06	1.13E-05	Median	2.734E-16	1.92E-16	5.03E-16
Variance	3.92E-11	4.41E-11	2.26E-10	Variance	2.944E-26	3.58E-26	2.111E-25
Kurtosis	3.02E+00	4.78E+00	3.07E+00	Kurtosis	6.57E+01	2.73E+02	1.40E+02
Skewness	1.36E+00	1.65E+00	1.63E+00	Skewness	6.69E+00	1.17E+01	1.02E+01
Pore Area Statistics				Throat Area Statistics			
	BANDERA GRAY	PARKER	BOISE		BANDERA GRAY	PARKER	BOISE
Mean	9.83E-09	8.38E-09	7.68E-09	Mean	4.18E-10	4.48E-10	1.548E-09
Min	0.00E+00	0	0.00E+00	Min	4.14E-13	4.14E-13	5.126E-13
Max	5.32E-07	7.79E-07	5.55E-07	Max	8.08E-09	9.97E-09	3.272E-08
Median	2.21E-10	1.74E-10	3.43E-10	Median	2.27E-10	2.33E-10	4.026E-10
Variance	1.14E-15	1.07E-15	8.22E-16	Variance	3.49E-19	4.92E-19	8.499E-18
Kurtosis	4.13E+01	6.63E+01	6.91E+01	Kurtosis	2.85E+01	4.11E+01	2.14E+01
Skewness	5.54E+00	6.62E+00	7.17E+00	Skewness	4.13E+00	5.08E+00	3.96E+00

Table 4-8: Ct Scan data summary after removing the zero values for pore radius and coordination numbers

Parameter			
	Boise	Bandera Gray	Parker
Porosity (fraction)	0.304	0.193	0.172
Number of pores (Body)	16294	14468	14199
Number of pores (Throats)	9162	7247	5521
Avg. coordination number	4.47	6.91	7.02
Smallest coordination number	1.0	1.0	1.0
Largest coordination number	39.0	31.0	32.0
Avg. pore radius (μm)	10.57	8.89	7.66
Largest pore radius (μm)	137	94.2	123
Smallest pore radius (μm)	1.04	0.93	0.93
Median pore radius (μm)	4.93	4.06	3.60
Avg. throat radius (μm)	16.23	9.69	9.93
Largest throat radius (μm)	102	50.7	56.3
Smallest throat radius (μm)	0.40	0.36	0.36
Median throat Radius (μm)	11.3	8.50	8.62

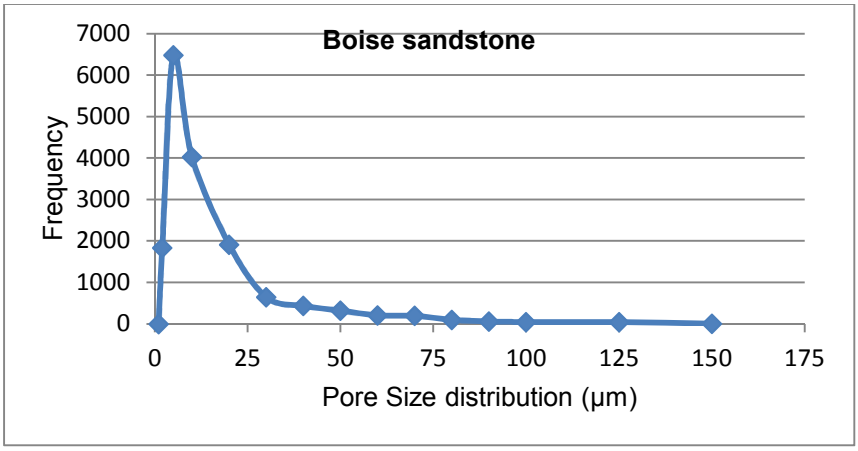

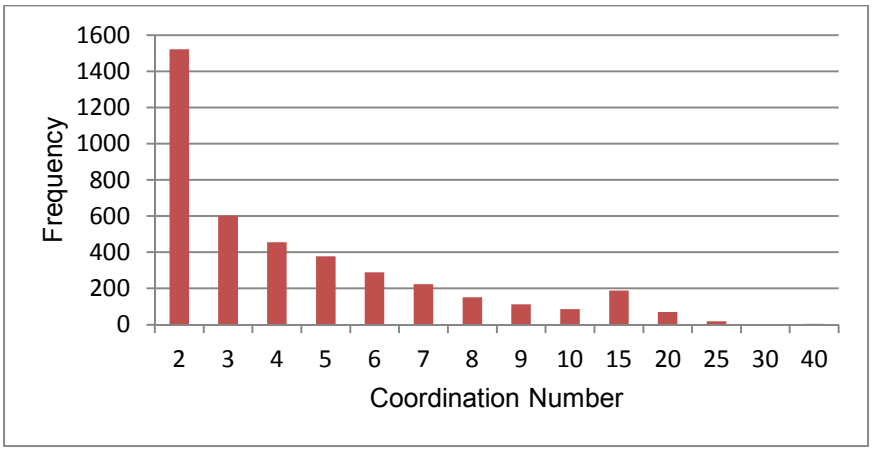

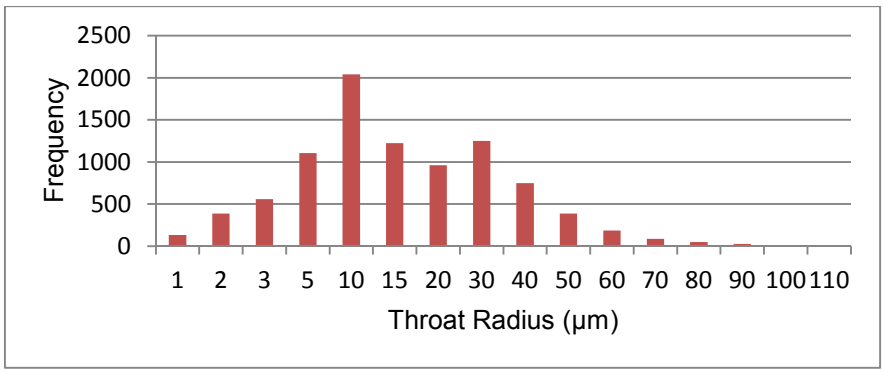

Figure 4-6: CT scan results for Boise sandstone: (a) pore size distribution from XCT Eqdiameter (top); (b) coordination number distribution (middle); and (c) pore throat distribution (bottom)

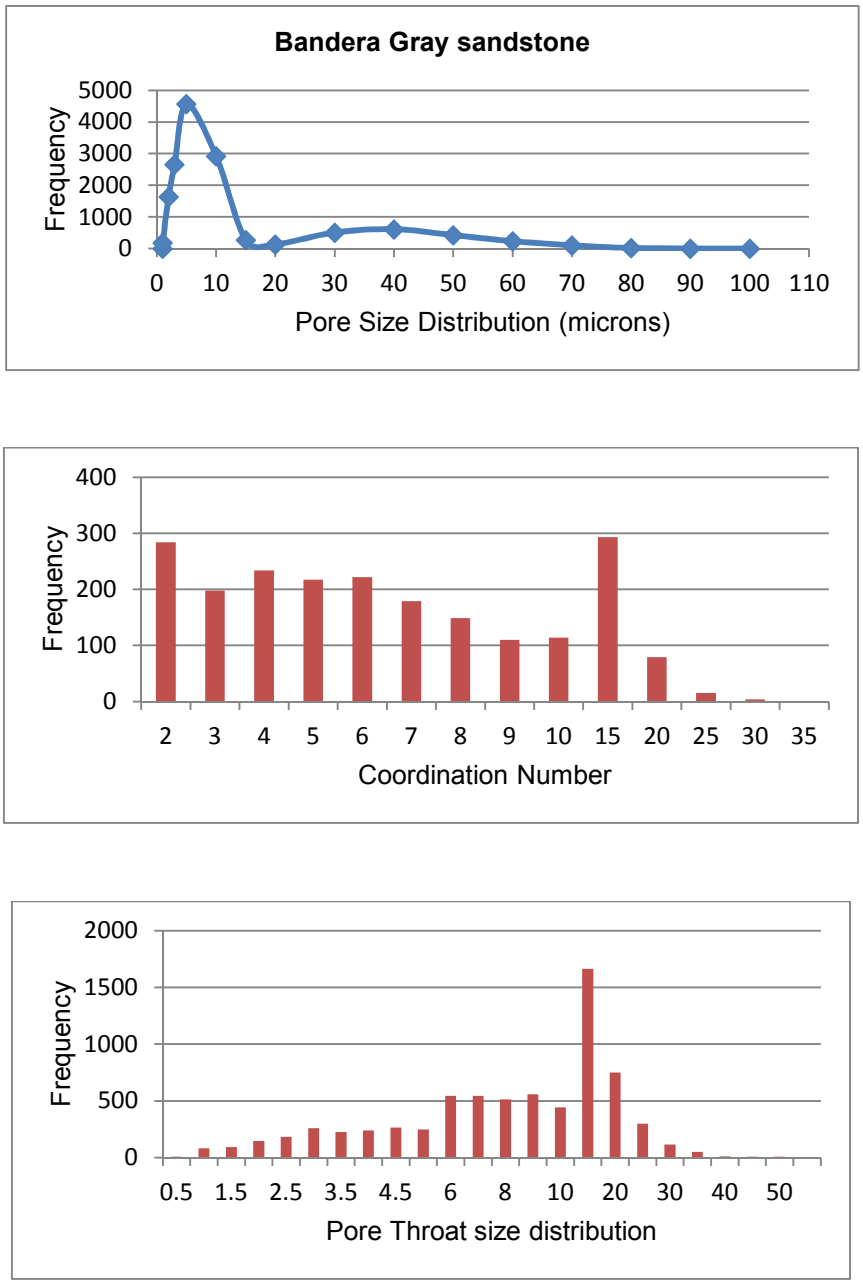

Figure 4-7: CT scan results for Bandera Gray sandstone: (a) pore size distribution from XCT Eqdiameter (top); (b) coordination number distribution (middle); and (c) pore throat distribution (bottom)

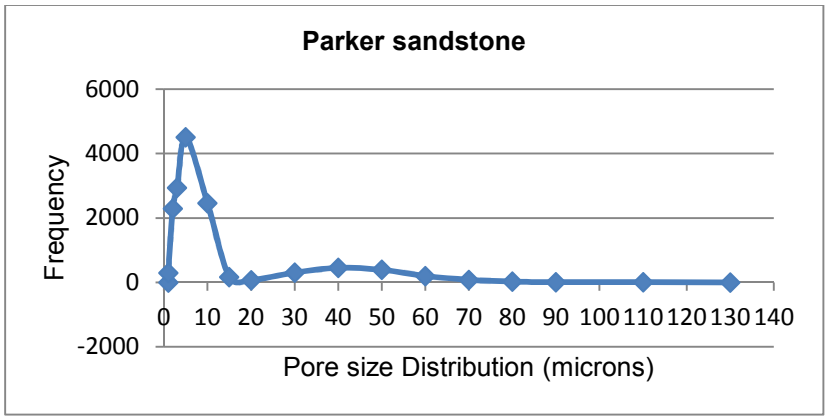

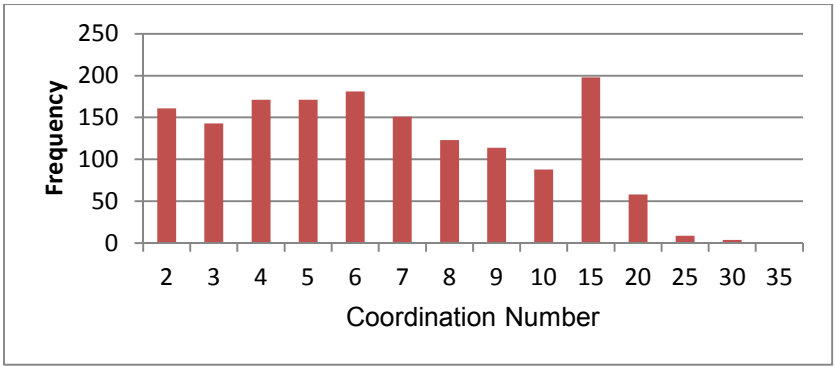

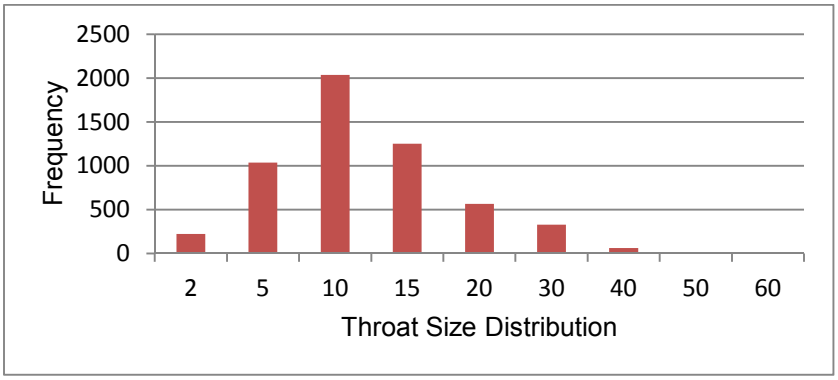

Figure 4-8: CT scan results for Parker sandstone: (a) pore size distribution from XCT Eqdiameter (top); (b) coordination number distribution (middle); and (c) pore throat distribution (bottom)

4.4 Fluid Imbibition:

For spontaneous fluid imbibition using DI water, the cumulative imbibition height and imbibition time is plotted on a log-log scale (e.g., Figure 4-9 for Parker sandstone) for all samples to obtain the imbibition slopes that are compiled in Table 4-10. All samples develop a steep (imbibition slope >1) initial phase of imbibition for <30 seconds (e.g., Figure 4-9). This is likely due to the rapid water imbibition along the sample wall and well-connected edge-accessible pore spaces of limited distance into the sample interior. Once these pore spaces are saturated, this initial phase is followed by water imbibition into the sample interior from capillary pressure gradient. For the cylinder samples (except for Gray Berea sandstone), this subsequent intermediate-time stable slope of 0.5 and above was observed (Figure 4-9). This half-slope value, with the imbibition proceeding in a square-root-time relationship, is an indication of high connectivity for the pores of samples for this sample (size) system (Hu et al., 2012)

Table 4-9: Water imbibition slopes for all samples.

Sample	Cylinder	Cylinder	Cube	Cube imbibition slope		
name	Bottom cross-sectional area (cm^2)	imbibition slope	Bottom cross-sectional area (cm^2)	Run 1	Run 2	Run 3
Idaho Gray	11.29	0.736	1.10	0.214	0.295	0.096
Boise	11.10	0.629	1.08	0.216	0.167	0.065
Gray Berea	11.46	0.386	1.08	0.156	0.288	0.140
Bandera Gray	11.10	0.537	1.01	0.270	0.109	0.332
Parker	11.10	0.519	1.21	0.303	0.228	0.206
Kentucky	11.10	0.636	1.11	0.344	0.303	0.120
Crab Orchard	11.10	0.504	1.14	0.325	0.360	0.313

Figure 4-10 shows the imbibition results for the same Parker sandstone, but on a

smaller-sized cube sample on which triplicate imbibition tests were conducted. The initial brief phase for cube sample has a >1 imbibition slope, just like the cylinder one. However, a follow-on reduced slope of about 1/4 is consistently seen for all cube-sized sandstone samples (Table 4-9). These results indicate that, overall, these sandstones have a relatively limited pore connectivity, which is manifested in cube imbibition tests with a smaller cross-sectional area for imbibition in the bottom face. For a sample with a specific pore connectivity, a larger imbibing area (e.g., plug in this work) will quickly lead water molecules to find the connected pore systems to have a classical (square-root-of-time relationship) imbibition behavior. However, for a smaller imbibition area, water molecules will have a higher tendencies to encounter into closed pore spaces, thus take a longer time (with an imbibition slope of 1/4) to reach the same distance.

Finally a typical flattening imbibition with extremely reduced slope (close to zero) is observed for very permeable samples within a short experimental duration (for example, in Figure 4-11 for Idaho Gray sandstone). This near-zero slope means that the wetting front has reached the sample top (the upper boundary), with a negligible capillary pressure gradient to imbibe more water. This slope is not considered and included in Table 4-9

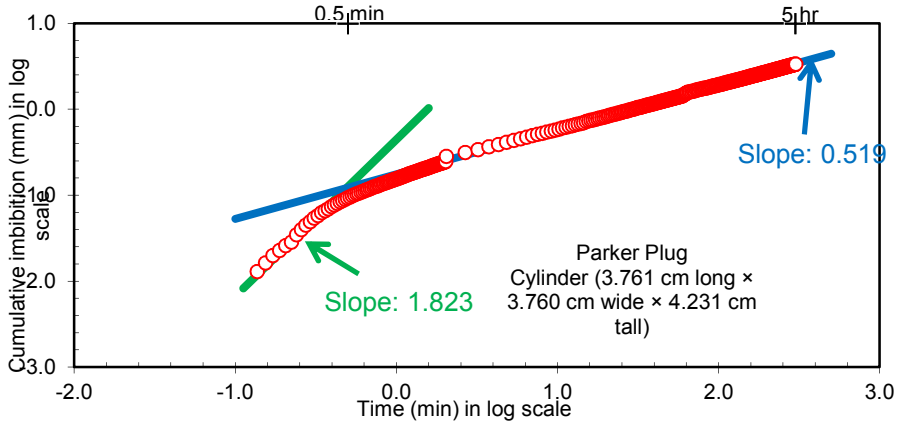

Figure 4-9: Parker cylinder plug showing a typical Fickian slope

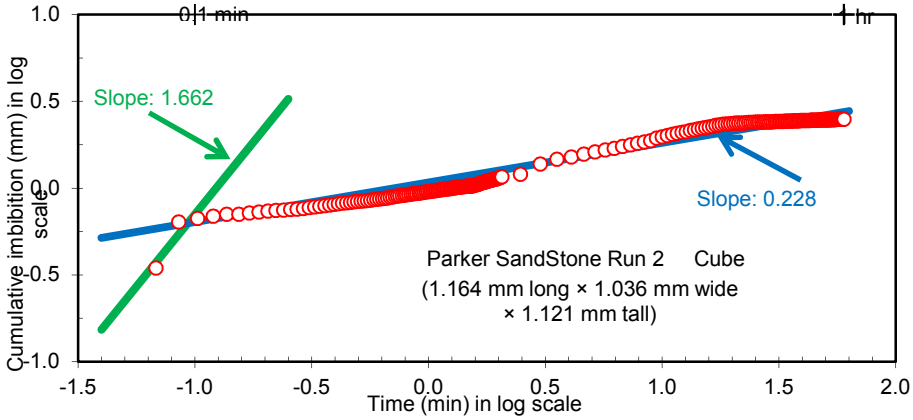

Figure 4-10: Typical imbibition behavior for cube sample (Parker sandstone) with less contact area for imbibition

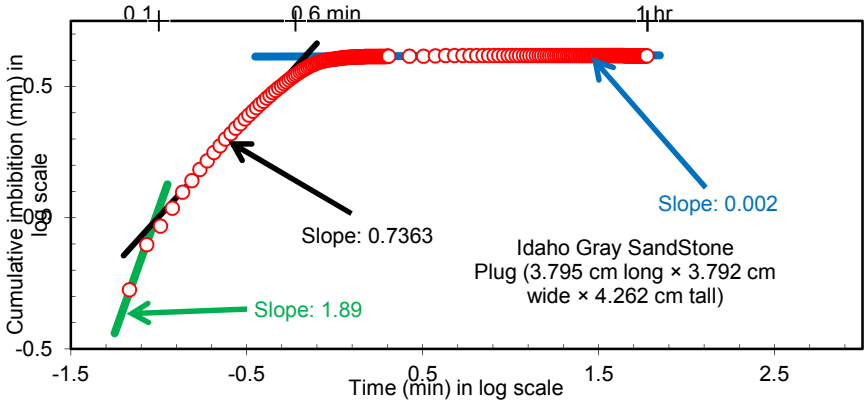

Figure 4-11: Idaho Gray imbibition slope showing all three phases.

The decrease in slopes to 0.25 could be attributable to either percolation threshold or reduced cross sectional area. In the samples tested, percolation threshold was not an issue because all samples have high connectivity; reduction in slopes especially in the cube samples could be a reflection of the area available for imbibition, as the wider cylinder samples have a larger bottom area and better chance for the fluid to find connected pore spaces (Table 4-9).

4.5 General Discussion:

4.5.1 Pore structure:

Pore structure (geometry and connectivity) of reservoir rocks, especially clastics, is dictated and affected by sedimentation and depositional environment to create primary porosity, and diagenesis to generate secondary porosity. Where the pores are connected, permeability or capacity for fluid flow is generated.

Pore structure is generally defined as throats and pore bodies, their sizes and connection. These throats and bodies can be further affected by different types of cementation materials, especially clays. These pore-bridging clays like the swelling montmorillonite (smectite) and pore-wall lining clays like illite and kaolinite may make pores unavailable for reservoir storage of hydrocarbon and even reduce permeability and production.

Several pore connectivity parameters, like coordination numbers, aspect ratio, equivalent diameter and pore surface to volume ratio, have been used to further clarify and delineate pores from throats. Several tools and techniques have been created to identify all these salient parts and paths of the pore structure in other to have a clearer picture. MICP, NMR, Micro Ct Scan are some of the tools available for pore structure or connectivity analysis and have been applied in this study. Their differences in principles and techniques may help to explain slight variations in results generated. Important things to understand regarding the tools are (1) expected results from tools; (2) procedures and techniques used in tools, and (3) finally limitations of each tool that applies to the concept of pore structure study.

4.5.2 Pore structure characterization from MICP:

MICP for instance has been applied and generally accepted as a common tool for pore structure study. Its applications include capillary pressure trend study, wettability

analysis, reservoir evaluation, and reservoir depletion. The small size of pores that could be enumerated from mercury injection has even found applications in reservoir seal capacity studies.

Mercury Injection is however limited by the size of pores it can enumerate (3 nm) due to equipment pressure and volume limitation. So any pores smaller than 3 nm are not expected to be seen. Based on this limitation, mercury injection may not be applicable to nuclear waste re-injection study into solid reservoirs with pores smaller than 3 nm. Secondly, mercury injection identifies pore throats rather than pore bodies. So it does not provide the complete picture of the pore structure of a rock. Thirdly the algorithm used for data reduction is based on the assumption of a parallel capillary bundle of tubes, while in reality pore systems are composed of intricate systems of interconnected and tortuous paths. Finally mercury intrusion test is destructive and samples can no longer be re-used. There is also a disposal hazard posed as mercury vapor is highly toxic.

4.5.3 Pore structure characterization from NMR:

NMR has been known to provide lithology independent porosity, pore fluid typing and system analysis in oil and gas reservoir evaluation (Kenyon et al., 1995; Alvarado et al., 2003). Like MICP, NMR algorithm is based on the concept of parallel bundle of capillary tubes rather than the intricate paths involved in actual pore structure. It does identify pore bodies rather than pore throats. This means that it cannot provide the complete pore structure information when the approach is used alone. Finally the porosity provided by NMR, which is defined as area under the T_2 curve shape, is limited by the Time-to-Echo (TE) values. The shorter the TE value, the more representative the porosity information that will be generated. This effect is illustrated in figure 4-12 (from Green

Imaging Technologies, the manufacturer of Oxford instruments), which shows three T_2 distributions obtained on the same core sample.

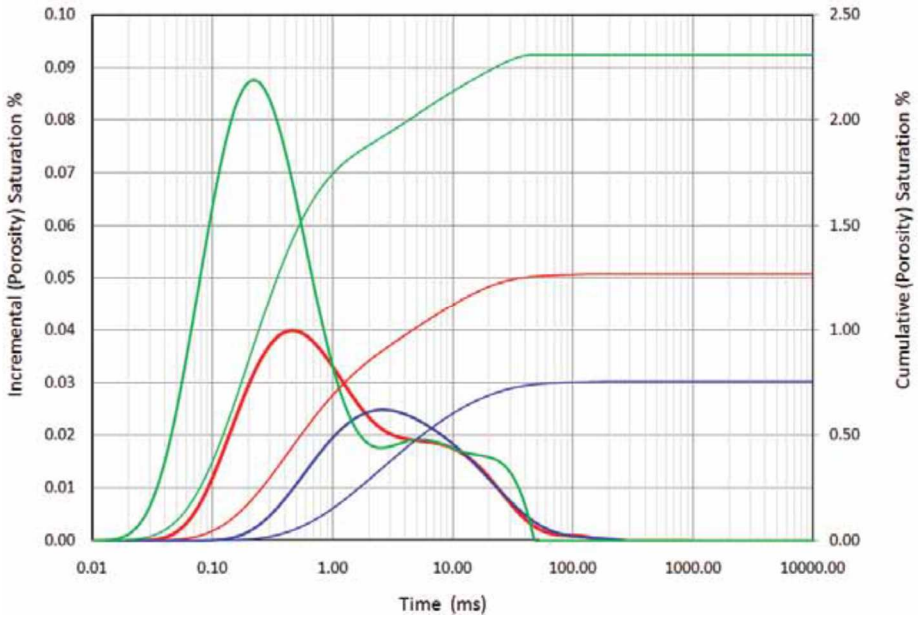

Figure 4-12: Comparing the effect of TE on porosity.

It is clear that the green (TE=100 μs) and the red (TE=200 μs) distributions show more detail at the shorter T_2 values (smaller pores) than does the blue distribution (TE=600 μs). The green distribution also records a much higher total integral signal, corresponding to a higher porosity value. The implication for various TEs on generated porosity is depicted in Table 4-10 below.

Table 4-10: Implications of smaller TE on porosity.

Sample	TE (μs)	Acquisition Time (min)	Number of Scans	Signal to Noise Ratio	NMR Porosity (ml)
1-4R	100	2	80	220.18	4.248
	200	5.5	224	203.06	2.175
	600	21.5	864	200.16	1.151

4.5.4 Pore structure characterization from Micro Ct Scan:

Micro Ct Scanning provides sufficient spatial resolution to allow the imaging of pore spaces and matrix in rocks, and therefore provide pore structure characterization. Its objective is to obtain descriptive images of density variations within an object. This density variation can then be used to identify and separate pores from the rest of the matrix in the rock sample. The paper of Honarpour (1985, SPE 14272) provided a detailed discussion of various applications of Ct Scan in reservoir evaluation. Ct scan is currently the readily-available tool that can rapidly and non-destructively map the complete structure of pores.

Its limitations, however, lie in the resolution of scans, subjective selection of threshold grayscale and several processing algorithms out there. According to Dong et al. (2007), for example, media axis-based algorithms can capture interconnectivity of the pores but identifying the actual pores is a problem. In addition, maximal ball algorithm easily identifies pores but has difficulty in constructing throats because there may be many ways to connect pores by overlapping smaller spheres.

Despite these shortcomings, micro Ct Imaging methods still show the more realistic and complicated pore shapes, compared to the cylindrical geometry assumed in MICP and NMR.

4.6 Porosity:

Porosity is defined as the summation or volume of all the pores available in the sample as a fraction of the total bulk volume. Total porosity is where all the pores (whether connected or closed) are enumerated, while effective porosity is where the closed or non-connected pores (e.g., those occupied by clay bound water) are subtracted from total pores.

When the pores are connected by throats, they aid permeability. Although the numbers generated from all procedures utilized in this thesis compares favorably, the slight differences could be explained by the limitations involved in procedures as discussed below. A summary of porosity from all approaches applied is provided in Table 4.11 and a combined plot showing the closeness of the data is provided in Figure 4-13

Table 4-11: Compilation of porosity values from all tests

Sample name	Total Porosity (fraction)			
	Helium	NMR	CT Scan	MICP
Idaho Gray	0.332	0.328	NA	0.359
Boise	0.286	0.285	0.304	0.323
Gray Berea	0.206	0.201	NA	0.219
Bandera Gray	0.203	0.199	0.193	0.183
Parker	0.189	0.181	0.172	0.158
Kentucky	0.148	0.144	NA	0.161
Crab Orchard	0.074	0.073	NA	0.094

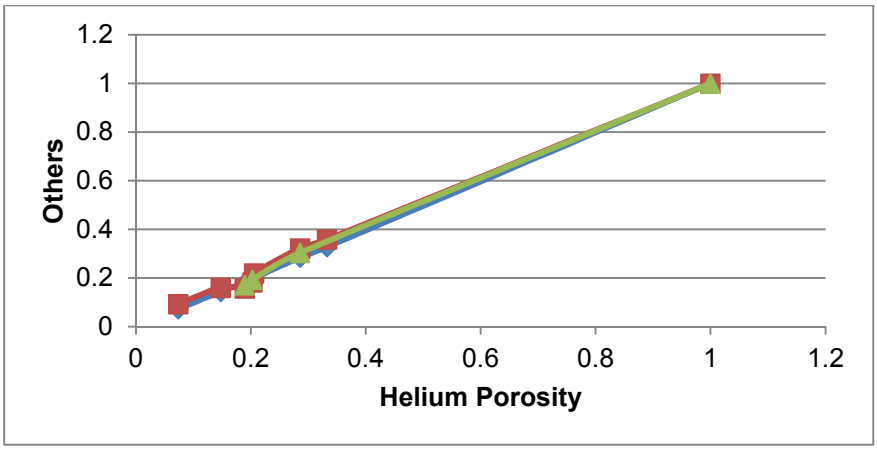

Figure 4-13: Comparison of helium porosity with other approaches

4.6.1 Helium porosity:

Helium porosity is generated using Boyle's law volume versus pressure, where the helium is expanded into a pre-weighed sample in a closed sample holder chamber from a helium tank on a pre-set pressure. The two key factors in helium porosity measurements are the accurate sample weight and sample being free from any moisture (API RP 40 standard).

Generated helium porosity is called total porosity because the sample has been dried using a conventional oven at 240 oF and helium was used as the percolating fluid. When dried in the oven at 240 oF, clay bound water in the sample is dried out and pores that otherwise may not be accessible are now accessible to be filled with helium. Helium is generally used because of its small molecule size, non-reactive nature and non-adhesion onto sample surfaces. Helium porosity is generally regarded as the benchmark or reference porosity.

4.6.2 MICP porosity:

Porosity from MICP is "total" but limited to accessible pore, so it is expected to be lower than helium porosity. When it is slightly higher, inappropriate conformance pressure or enumerating pores exposed to the outside and/or fracture may be responsible. The MICP porosity is, however, generally a reliable one to work with.

4.6.3 Nuclear Magnetic Resonance porosity:

As previously mentioned under pore structure discussion, porosity from NMR (when a sample is fully saturated with water) is defined as area under the T_{2s} curve, and is limited to TE and accessible pores. Where the T_2s curve does not represent all the T_2s present in the sample, then a signal from some pores will be missing and porosity will be under-reported. This situation can occur, for example, if the instrument being used is not

capable of detecting short T_2s signals from small pores, in which case porosity due to small pores will not be accounted for. Technically, this means that the instrument being used must be able to perform sustained measurements using short Time-to-Echo (TE) values. The shorter the TE value the more representative the porosity information that will be produced. TE values of 0.2ms was used for the NMR tests at Core Laboratories Facility in Houston. Minimum T_2s cutoff of 2.5 – 2.8ms is generally used to represent clay bound water pores. These are subtracted from "total" porosity to reflect "effective" porosity.

4.6.4 Micro Ct Scan porosity:

Although porosity from Micro Ct scan should be total and be more representative than other procedures, as previously mentioned, identification of pores/throats, coupled with gray scale subjectivity, plays a major role in the inconsistent numbers that could be generated.

4.7 Permeability:

Permeability is defined as the capacity of a rock layer to transmit water or other fluids, such as oil. The standard unit for permeability is the Darcy (d) or, more commonly, the millidarcy (md). Permeability is an important parameter for basin-scale fluid flow modeling, reservoir engineering, aquifer drawdown calculations, and wellbore stability. It is a function of the geometry of the pore structure of the porous media. Permeability is controlled in sandstone by grain size, grain orientation, packing arrangement, cementation, clay content, bedding, and grain size distribution and sorting. All these are factors that play prominently into the distribution of pore sizes.

Laboratory permeability measurements on porous media samples are straightforward, and only depend on fluid type, steady and unsteady measurement state,

and finally a set of Darcy rules that must be obeyed for laboratory measured permeability to be valid.

Several methods are currently available for estimating permeability from bulk physical properties and other petrophysical tools. One of the simplest permeability estimation methods assumes a log-linear relationship between permeability and porosity (Rose, 1945). Although this relationship varies greatly with lithology, it is generally accepted especially in clastics, and provide a quick method to assess the quality of the reservoir using a concept called reservoir quality index (RQI). A table of post-test porosity and permeability for set A samples is displayed below (Table 4-12) and followed by the classic porosity-permeability plot in Figure 4-14.

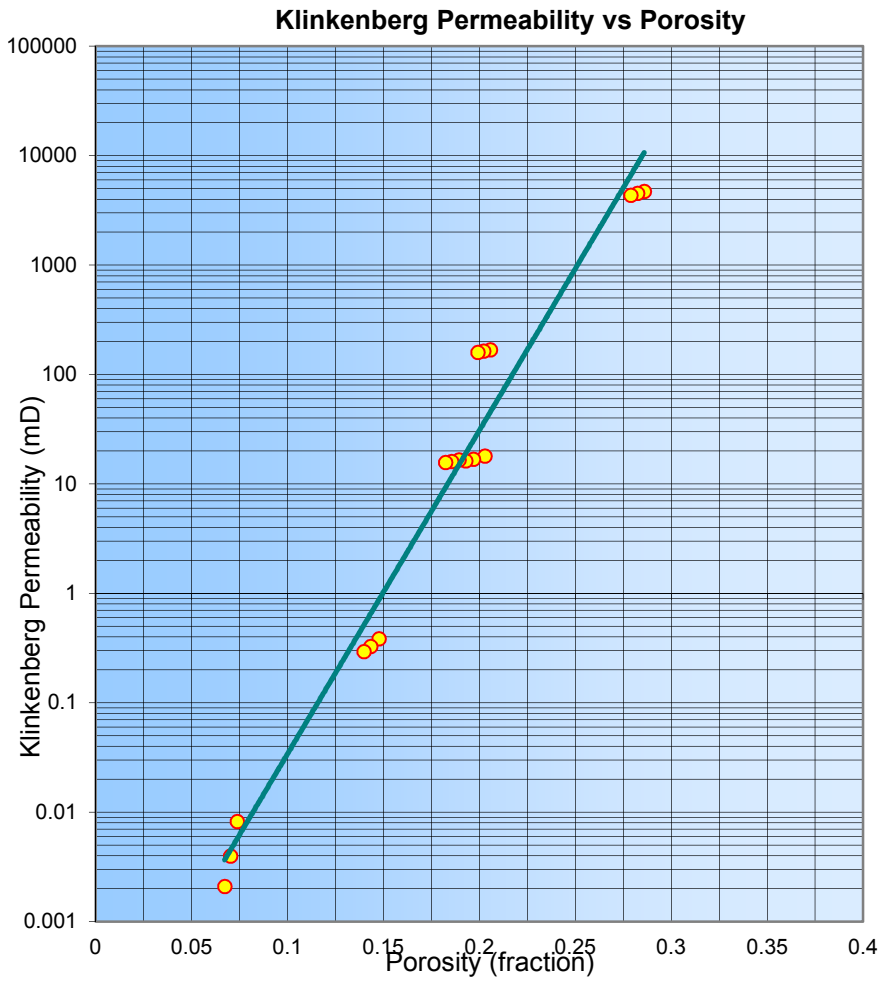

Figure 4-14: Classic porosity-permeability plot for reservoir quality index; note that Idaho Gray is not included in the plot

Table 4-12: Post-processing permeability and porosity at multiple stresses

Sample Number	Confining Stress psi	Porosity Helium fraction	Kinf md	Kair md
Idaho	800	0.332	-	> 50 Darcy
Gray	2000	0.327	-	> 50 Darcy
	4000	0.322	-	> 50 Darcy
Boise	800	0.286	4730.	4780.
	2000	0.282	4520.	4570.
	4000	0.279	4360.	4410.
Gray Berea	800	0.206	168.	176.
	2000	0.202	164.	171.
	4000	0.199	160.	167.
Bandera Gray	800	0.203	18.0	20.7
	2000	0.197	16.9	19.6
	4000	0.193	16.2	18.7
Parker	800	0.189	16.6	19.5
	2000	0.185	16.0	18.9
	4000	0.182	15.7	18.4
Kentucky	800	0.148	0.384	0.608
	2000	0.143	0.329	0.527
	4000	0.140	0.295	0.468
Crab Orchard	800	0.074	0.008	0.026
	2000	0.070	0.004	0.015
	4000	0.067	0.002	0.009

Other methods for permeability estimation utilize the theory of Kozeny, which states that permeability should be inversely proportional to the square of the specific surface area of the porous medium (Kozeny, 1927). More recent work has focused on grain shape (Schwartz and Banavar, 1989), pore shape (Yang and Aplin, 1998), and fluid pathways as they relate to percolation theory (Bryant et al., 1993) (all quoted by Daigle and Dugan, 2009). In all cases, knowledge of pore geometry, grain size, grain shape, and fluid pathway is integral to permeability evaluation. If these parameters are known, then permeability could be estimated with some degree of confidence.

In this work, permeability derived from all approaches are compared and results tabulated in Table 4.4 above. The discrepancies in the permeability results obtained from this thesis work might be due to different approaches and their inherent limitations. The permeability value for Idaho Gray of about 20-30 Darcy is only estimated because it is generally outside the measurable range of equipment used.

Helium or nitrogen, unsteady state, pressure draw-down permeability tests have been in use (with CMS-300 instrument) and accepted as the benchmark for pore connectivity studies in Core Laboratories since 1990 (Jones, 1990). It is generally run on a sample that has been oven dried at 240^{o}C. Again this means the clay bound water has been dried out and may connect some of the otherwise isolated pores.

Several algorithms, including Purcell, Thomeer, Katz and Thompson, and Swanson, have been applied to permeability estimation from MICP tests. All of them have their principles based on the bundle of capillary tubes theory and may be lower than helium permeability. Swanson as currently presented has been shown to be invalid in permeabilities lower than 0.01 md (Amaefule et al., 1997) and may not be applicable in shale or tight gas reservoir studies except if modified per Amaefule/Walls equation.

Permeability from NMR uses several algorithms including Coates, Modified Coates and SDR. So far SDR is the only one that can be estimated based on T_2 from fully saturated samples and it depends on the constant of correlation (c) and porosity.

Permeability from Ct Scan uses several algorithms including the use of Stokes equation but it requires a high intensive computer processing power and could not be completed in this work due to computing limitations.

Chapter 5

CONCLUSION

Despite different measurement principles, procedures and approaches, results from all methods complement each other and provide a clearer picture when it comes to determining pore size structure (pore size distribution, connection). The combination of Mercury intrusion porosimetry and NMR may provide a complete picture of pore structure if the potential pitfalls are properly addressed. Also where appropriate algorithms are applied, data from Micro Ct Scan might be able to provide a complete picture and serve as a stand-alone tool for pore structure analysis. A less subjective approach to accomplishing maximal gray scale in Ct Scan will also help boost the confidence in data reduction and image processing. Unfortunately, the short term temporary license provided for the software Avizo did not provide adequate time to properly learn and understand its full capabilities.

My conclusion is that all procedures tend to complement each other and sometimes serve as calibration or reference for data from different approaches.

Future work might include validating the extracted information from Ct scan and using it to predict permeability with Stokes equation and multiphase flow properties, such as relative permeability and capillary pressure. The derived NMR permeability using SDR can also be compared with the concept of Kozeny equation for permeability. Validation of correlation between pore-entry pressure in mercury intrusion and grain packing and sorting will be a welcoming idea especially for clastics.

References

Al-Khasuri, A.S., and Blunt, M.J. 2007. Network extraction from sandstone and carbonate pore space images. *Journal of Petroleum Science and Engineering*, 56: 219 – 231.

Appoloni C.R., Rodrigues C.R.O., Fernandes C.P. 2005. Porous microstructure characterization of a sandstone reservoir using high-resolution x-ray micro tomography. SCA 2005-41

Beckers E., Plougonven E., Roisin C., Hapca S., Leonard A., and Degre A. 2014. X-ray microtomography: A porosity-based thresholding method to improve soil pore network characterization. Geoderma 219–220: 145-154

Burdine, N.T., Gournay L.S., and Reichertz P.P. 1950. Pore size distribution of petroleum reservoir rocks. Petroleum Transaction, AIME, Vol 189.

Carlos A. Le´on y Le´on. 1998. New perspectives in mercury porosimetry, Advances in Colloid and Interface Science, 76-77: 341-372

Comisky J.T., Newsham K.E., Rushing J.A., and Blasingame T.A 2007. A comparative study of capillary-pressure-based empirical models for estimating absolute permeability in tight gas sands

Daigle H., and Dugan B. 2009: Extending NMR Data for permeability estimation in fine-grained sediments. Marine and Petroleum Geology 26: 1419 - 1427

Dong H., Touati M., and Blunt M.J. 2007: Pore Network Modeling. Analysis of Pore Size Distribution of Arabian Core Samples SPE 105156.

Ewing R.P., and Horton. R., 2002. Diffusion in sparsely connected pore spaces: Temporal and spatial scaling. *Water Resources. Res.*, 38: 1285, doi:10.1029/2002WR001412

Gallegos, D. P., and D. M. Smith. 1988. A NMR Technique for the Analysis of Pore Structure: Determination of Continuous Pore Size Distributions, *J. Colloid Interface Sci.,* 122**,** 143.

Gao, Z.Y., and Q.H. Hu. 2013. Estimating permeability using median pore-throat radius obtained from mercury intrusion porosimetry, J. Geophysical Engineering. **10** (2013) 025014 (7pp)

Giesche, H., Mercury Porosimetry: A General (Practical) Overview, WILEY-VCH verlag GmbH & Co KGaA, Weinheim

Honarpour M.M., and Cromwell V., (1985): Reservoir Rock Descriptions using Computed Tomography, SPE 14272

Hu Q.H., Ewing R.P., and Dultz S.,(2012): Low pore connectivity in natural rock, Journal of Contaminant hydrology

Kamath, J., (1992): Evaluation of Accuracy of Estimating Air permeability from Mercury Injection Data. *SPEFE*, p 304-310.

Lenormand, R., Interpretation of mercury injection curves to derive pore size distribution, SCA 2003-52

Li aw, H.K., Kulkarni, R., Chen, S., and Watson, T.A, The use of Magnetic Resonance Spectroscopy to probe microscopic structures and fluid distributions in porous media, SCA 9403

Looyestijn. W.J., (2001): Distinguishing fluid properties and producibility from NMR logs, proceedings of the 6th Nordic symposium on petrophysics, 15-16 May, Trondheim, Norway.

Ma S., and Morrow N.R., (1996): Relationship between Porosity and Permeability for Porous Rocks, international Symposium of the Society of Core Analysts, Sept. 8-10, Montpelier, France.

Marschall, D., Gardner, J. S., Mardon D., Coates, G.R.,(1995): (NUMAR Corp., Houston, TX): Method for correlating NMR relaxometry and mercury injection data, SCA Conference Paper Number 9511

Peng S., Marone F., and Dultz S., (2014): Resolution effect in x-ray micro computed tomography imaging and small pore's contribution to permeability for a Berea Sandstone. Journal of Hydrology 510 403-411

Peng S., Hu Q., Dultz S., and Zhang M.(2012): Using x-ray micro computed tomography in pore structure characterization of a Berea Sandstone: Resolution effect. Journal of Hydrology 472-473 (2012) 254-261

Rabbani S., Jamshidi S., and Salehi S., (2014): An automated simple algorithm for realistic pore network extraction from micro tomography images, Journal of Petroleum Science and Engineering 123 164-171

Schon J.H., (2011): Physical properties of Rocks: Workbook

Sorland G.H., Djurhuus K., Lien J.R., and Skauge S., (2006) Absolute pore Size Distribution from NMR SCA

Straley, C., Rossini, D., Vinegar, H., Tutunjian., P., Morris C. Core Analysis by Low Field NMR, SCA 9404

Swanson B.F.,(1981) A Simple Correlation between Permeabilities and Mercury Capillary Pressures, *Journal of Petroleum Technology*, December 1981, p 2498-2504

Yan, Z., Chen, C., Fan, P., Wang, M., Fang, X. (2015) Pore structure Characterization of Ten Typical Rocks in China, EJGE, Vol 20, 2015

Biographical Information

Samson S. Arawole's academic career at University of Texas at Arlington was as challenging as is rewarding. He finally completed his thesis and earned his Master's degree in Geology after so many detours. Now it's time to focus on fully improving himself in the Oil and gas industry and the market-place in general. He knows and believe real life learning just began.

The thesis project provided an opportunity for him to have an independent learning process beyond the scope of classroom lectures, for the various technologies involved. He now has a better understanding of applications of NMR, Micro Ct Scan, Mercury Injection Capillary pressure and Fluid imbibition technologies and their scientific procedures.

Thank you UTA and all Geoscience faculty staff especially Dr. Wickham for providing the enabling environment.